Forearc motion and deformation between El Salvador and Nicaragua: GPS, seismic, structural, and paleomagnetic observations

D. Alvarado[1]*, C. DeMets[1], B. Tikoff[1], D. Hernández[2], T.F. Wawrzyniec[3†], C. Pullinger[4], G. Mattioli[5§], H.L. Turner[5], M. Rodriguez[6], and F. Correa-Mora[1]*

[1]DEPARTMENT OF GEOSCIENCE, UNIVERSITY OF WISCONSIN–MADISON, MADISON, WISCONSIN 53706, USA
[2]SERVICIO NACIONAL DE ESTUDIOS TERRITORIALES, SAN SALVADOR, EL SALVADOR
[3]EARTH AND PLANETARY SCIENCES, UNIVERSITY OF NEW MEXICO, ALBUQUERQUE, NEW MEXICO 87131, USA
[4]LAGEO, 15 AVENIDAS SUR, COLONIA UTILA, SANTA TECLA, LA LIBERTAD, EL SALVADOR
[5]DEPARTMENT OF GEOLOGY, UNIVERSITY OF ARKANSAS, FAYETTEVILLE, ARKANSAS 72701, USA
[6]ESCUELA DE FISICA, UNIVERSIDAD NACIONAL AUTONOMA DE HONDURAS, BULEVAR SUYAPA, TEGUCIGALPA, HONDURAS

ABSTRACT

We combine geodetic, structural, and paleomagnetic data from El Salvador with Global Positioning System (GPS) data from southern Honduras and Nicaragua to describe the motions of the Salvadoran and Nicaraguan forearcs and determine the location and style of faulting across the Gulf of Fonseca offset of the volcanic arcs of eastern El Salvador and western Nicaragua. Finite-element modeling of GPS measurements at 35 sites in El Salvador, southern Honduras, and Nicaragua indicates that the Nicaraguan and Salvadoran forearcs both move west to northwest, parallel to their respective trenches, at 15 ± 2 mm yr^{-1} (95% limit) in a Caribbean plate reference frame. The similar motions of the two forearcs, despite an ~20°–25° difference in the obliquity of subduction beneath them and absence of any significant convergence obliquity offshore from El Salvador, are consistent with a recent hypothesis that the Nicaraguan forearc pushes the Salvadoran forearc to the northwest, possibly driven by northwestward lateral escape of the Central America forearc from its collision zone with the Cocos Ridge offshore from Costa Rica. The Gulf of Fonseca and adjacent eastern El Salvador form an ~60-km-wide extensional zone with E-W elongation, determined by diffuse seismicity, GPS velocities, and numerous young, N-S–striking normal faults mapped with a 10 m digital elevation model (DEM), structural measurements, and Lidar (light detection and ranging). Strike-slip earthquakes in the Fonseca pull-apart structure and evidence for modest (~10°) vertical-axis fault block rotations from paleomagnetic measurements at 33 sites in the Fonseca pull-apart structure both indicate that extension may be accompanied by bookshelf faulting.

LITHOSPHERE; v. 3; no. 1; p. 3–21; Data Repository 2011053. doi: 10.1130/L108.1

INTRODUCTION

Geological and geophysical data convincingly establish that oblique subduction along many plate margins is partly or fully partitioned into a trench-parallel component that induces the coastwise transport of forearc slivers and a trench-normal component that is accommodated by less oblique subduction. Fitch (1972) was the first to describe the tendency for shallow, subduction-thrust earthquakes along many subduction zones to have slip directions intermediate between the direction orthogonal to the trench and the convergence direction estimated from plate motion models. He attributed this to trench-parallel movement of forearcs with respect to interior areas of the overlying plate. Numerous subsequent authors have considered the ways in which forearcs respond to changes in the obliquity of subduction or degree of partitioning along a trench (e.g., Jarrard, 1986; Kimura, 1986; Avé Lallemant and Guth, 1990; Beck, 1991; McCaffrey, 1992). For example, changes in obliquity along a trench due to either convex and concave bends in the trench or gradual along-strike changes in plate convergence velocities may induce trench-parallel extension or shortening of the forearc (Fig. 1). Manifestations of these along-strike changes in partitioning can include large-scale, vertical-axis block rotations (Beck, 1991), sliver fragmentation and rotation of the resulting blocks (Geist et al., 1988), exhumation of high-pressure rocks (Avé Lallemant and Guth, 1990), and along-strike variations in the amount of extension and contraction (McCaffrey, 1996).

A major concave bend in the Middle America Trench occurs off the Pacific coast of Nicaragua (Fig. 1), where the Cocos plate subducts northeastward beneath the western edge of the Caribbean plate at rates of 75–85 mm yr^{-1}. Offshore from southeastern Nicaragua, where Cocos plate convergence is ~20°–25° counterclockwise from the direction normal to the trench (Fig. 1), an ~10° deflection of the average direction of shallow thrust earthquakes toward trench-normal (DeMets, 2001, 2002; LaFemina et al., 2009) is consistent with partial partitioning of the oblique convergence and 14 ± 2 mm yr^{-1} of northwestward forearc translation (DeMets, 2001). Moderate magnitude ($M \leq 6.5$) sinistral strike-slip earthquakes on arc-transverse faults along the Nicaraguan volcanic arc (LaFemina et al., 2002; Funk et al., 2009) were interpreted by LaFemina et al. (2009) as evidence for bookshelf faulting along the volcanic arc in response to NW-directed movement of the forearc (Fig. 1), offering independent evidence for this partitioning. Global Positioning System (GPS) measurements at stations in the Nicaraguan forearc confirm that the forearc moves to the NW at

*Current address: Chevron USA, 1500 Louisiana St., Houston, Texas 77002, USA
†Current address: Geology Program, Western State College of Colorado, Gunnison, Colorado 81231, USA
§Current address: Department of Earth and Environmental Sciences, University of Texas, Arlington, Texas 76019, USA

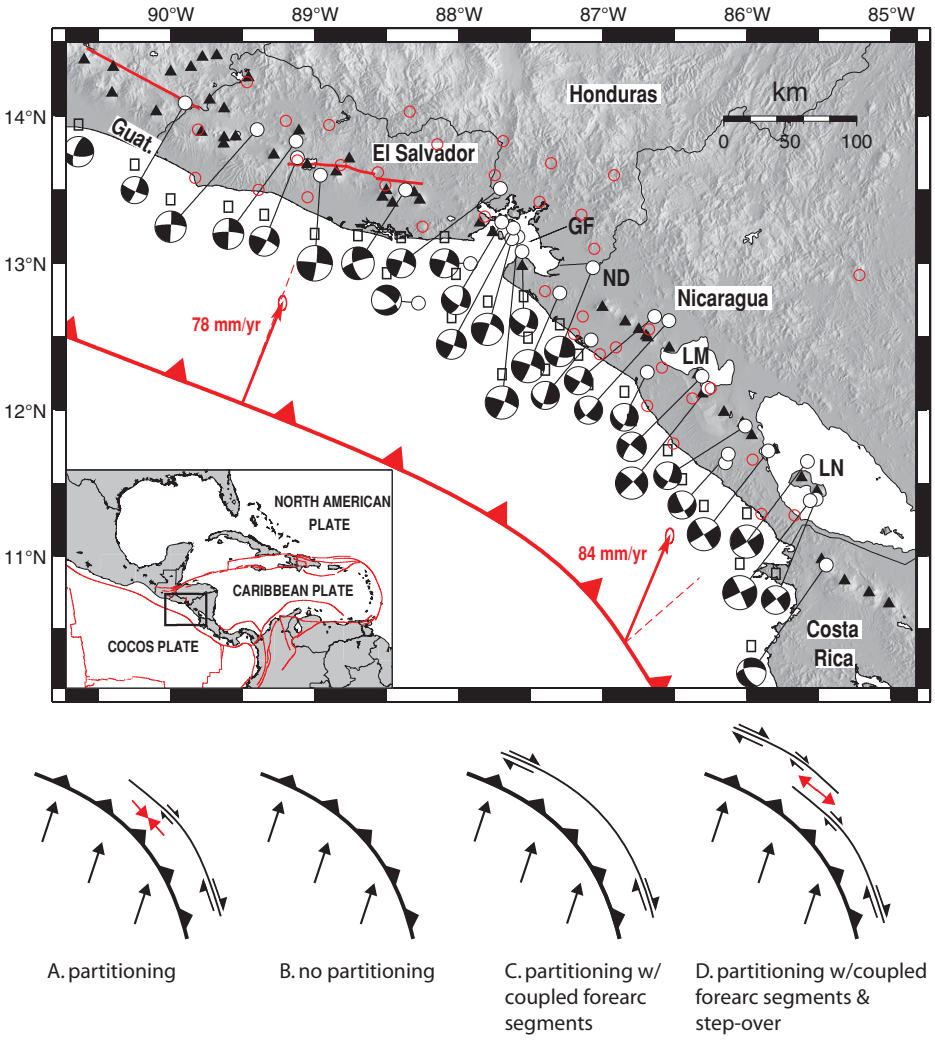

Figure 1. (Upper panel) Tectonic and topographic map of study area showing major plate boundaries (red lines), focal mechanisms of shallow-depth earthquakes within the Caribbean plate, and locations of Global Positioning System (GPS) stations used in this study (red circles). Inset in lower left corner indicates location of study area (black square) and names of tectonic plates. Topography is from 30 m Space Shuttle Topographic Radar Mission (SRTM) data. Red arrows and ellipses show Cocos plate velocities relative to Caribbean plate and 1σ uncertainties (DeMets, 2001). Red dashed lines indicate directions perpendicular to the trench. Black triangles represent active volcanoes. Focal mechanisms are from the Global Centroid Moment Tensor (CMT) catalog and sources given by DeMets (2001). GF—Gulf of Fonseca; ND—Nicaraguan Depression; LM—Lake Managua; LN—Lake Nicaragua. (Lower panel) Idealized forearc deformation along a concave-shaped subduction zone, as follows: (A) Convergence obliquity and partitioning of oblique convergence decrease from southeast to northwest and induce local, margin-parallel shortening (red arrows) with variable strike-slip component in the forearc. (B) Weak or zero coupling across a subduction interface gives rise to no slip partitioning and hence no upper-plate deformation. (C) Undeformed forearc translates along the trench if coupling is weak and forearc motion is driven by push or pull beneath or at the trailing or leading edge of the forearc. (D) Same as C, but with localized extension (red arrows) at an offset of the overlying forearc fault. Black arrows indicate relative plate motion.

rates of 10–15 mm yr^{-1} relative to the Caribbean plate (Turner et al., 2007).

In contrast to Nicaragua, the Cocos-Caribbean subduction direction off the coasts of El Salvador and northwestern Nicaragua is nearly orthogonal to the trench (Fig. 1; DeMets, 2002). Little or no movement of the Salvadoran forearc is thus expected if partitioning of oblique convergence is the only process capable of moving the forearc parallel to the trench. Contrary to this expectation, a series of active strike-slip faults, named the El Salvador fault zone by Martínez-Díaz et al. (2004), follows the Salvadoran volcanic arc and exhibits right-lateral offsets of Holocene-age features at an average slip rate of 11 mm yr^{-1} (Corti et al., 2005). Consistent with these offsets, GPS stations on the Salvadoran forearc move faster than 10 mm yr^{-1} westward relative to sites inland from the volcanic arc (Fig. 2; Correa-Mora et al., 2009), and moderate-magnitude, dextral strike-slip earthquakes accommodate WNW-directed slip along the El Salvador fault zone (Fig. 1; White, 1991; White and Harlow, 1993). Compelling evidence thus exists for westward motion of the Salvadoran forearc despite the absence of oblique subduction offshore.

These observations raise several questions about the forearc kinematics between Costa Rica and Guatemala. Do the Salvadoran and Nicaraguan forearcs move with respect to each other, as might be expected given the ~20° difference in the obliquity of Cocos plate convergence beneath them (Fig. 1)? Why does the Salvadoran forearc translate along the trench given that subduction is orthogonal and coupling across the subduction interface is weak or zero (Correa-Mora et al., 2009)?

Related to these questions, how is motion in central Nicaragua, where faults in the Nicaraguan depression accommodate motion of the forearc sliver (Cowan et al., 2002; LaFemina et al., 2002), transferred to the El Salvador fault zone through the poorly understood Gulf of Fonseca (Fig. 1)? The gulf is a shallow, seismically active embayment located at the junction of the Nicaraguan and Salvadoran forearcs (Funk et al., 2009). Across the gulf, the volcanic arc shifts ~40 km inland and bends ~20° counterclockwise, mirroring the concave bend in the trench farther south. Plausible hypotheses for deformation across the Gulf of Fonseca include at least the following: (1) deformation is focused along a narrow fault zone (Fig. 3A); (2) deformation is distributed across an extensional step-over of the volcanic arc faults (Fig. 3B); and (3) trenchward escape of the NW-translating Nicaraguan forearc sliver gives rise to a zone of extension at the northwest termination of the Nicaraguan forearc (Fig. 3C). Resolution of these options is critical for a better understanding of the nature of the kinematic link between the two forearcs.

Herein, we treat these questions by combining new regional- to outcrop-scale structural observations from eastern El Salvador with recently published GPS station velocities from El Salvador (Correa-Mora et al., 2009), Honduras (Rodriguez et al., 2009), and Nicaragua (Turner et al., 2007). To establish the necessary kinematic framework for interpreting the structural observations, we first use the GPS station velocities to determine best-fitting rates of trench-parallel translation for the Nicaraguan and Salvadoran forearcs and test for motion between them. We then describe and interpret

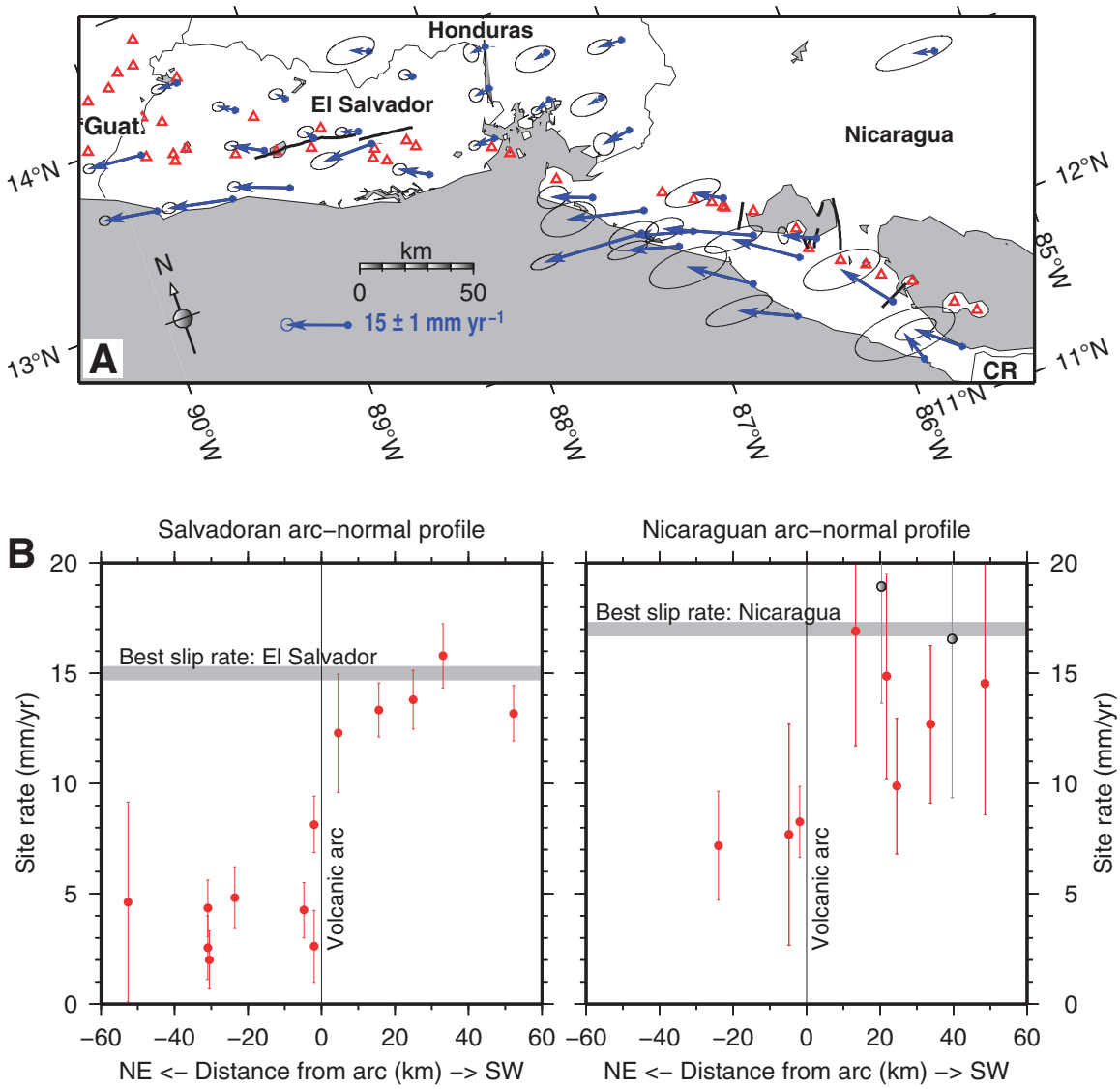

Figure 2. (A) Oblique Mercator projection of Global Positioning System (GPS) station velocities in the study area relative to a stationary Caribbean plate. Ellipses show two-dimensional (2-D) 1σ velocity uncertainties. Red triangles show volcano locations. Abbreviations: CR—Costa Rica; Guat.—Guatemala. (B) Variation of GPS station rates in El Salvador (left) and Nicaragua (right) with distance from nearby volcanic arc faults. The distance from a given GPS site to the nearest strike-slip fault is measured along a great circle that strikes N06°E in El Salvador and N41°E in Nicaragua. Shaded horizontal lines indicate the best-fitting forearc slip rates estimated from the GPS velocity inversions described in the text. The 15 mm yr^{-1} and 17 mm yr^{-1} rates that best fit the Salvadoran and Nicaraguan GPS site velocities, respectively, differ insignificantly from the 15 mm yr^{-1} rate that results from a simultaneous inversion of both sets of velocities. Gray circles in B indicate GPS sites that were occupied only twice and for which both the rates and uncertainties are more poorly known than for the other sites. All other stations included in the study were occupied three or more times.

our new structural observations, which consist of paleomagnetic, structural, topographic, and Lidar (light detection and ranging) data, and $^{40}Ar/^{39}Ar$ age dates from eastern El Salvador near the Gulf of Fonseca. The body of structural and geodetic evidence leads to a surprisingly simple model for the recent tectonics and kinematics of the Central American forearc, with important implications for our understanding of the forces that are responsible for deformation along much of the Pacific coast of Central America.

GPS SITE VELOCITIES AND UNCERTAINTIES

The GPS velocities used for our analysis were derived from campaign and continuous measurements made since 1999 at 35 stations in El Salvador, southern Honduras, and Nicaragua, (Fig. 2). Further information about the GPS data and methods for processing them may be found in the GSA Data Repository.[1] Readers are also referred to Rodriguez et al. (2009) and Turner et al. (2007) for more information about the Honduran and Nicaraguan station velocities, respectively. Descriptions of any corrections we made to the GPS coordinate time series for the coseismic and postseismic effects of regional

[1]GSA Data Repository Item 2011053, Figures DR1–DR3 and Table DR1, is available at www.geosociety.org/pubs/ft2011.htm, or on request from editing@geosociety.org, Documents Secretary, Geological Society of America, P.O. Box 9140, Boulder, CO 80301-9140, USA.

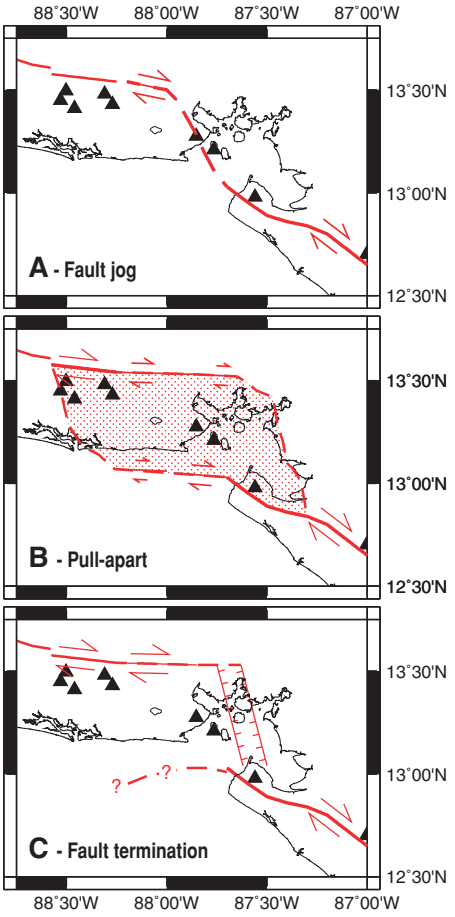

Figure 3. Schematic diagrams discussed in text for possible deformation across the Gulf of Fonseca in response to the offset of the volcanic arc and volcanic arc faults. Arrows indicate sense of relative motion across the faults, and triangles show volcano locations.

earthquakes are also found in the GSA Data Repository (see footnote 1).

The GPS station velocities described here are specified relative to the Caribbean plate interior. As described in the data repository supplement, the angular velocity that specifies motion of the Caribbean plate is estimated from the velocities of 17 GPS stations at various locations in the plate interior, including sites in eastern Honduras and Nicaragua, which constrain the plate motion close to the areas studied herein. The Caribbean plate reference frame differs little from that described by DeMets et al. (2007) and is not a limiting factor in any of the results described here.

Trench-Normal Component of Station Motion: Evidence for Weak Subduction Coupling

The most striking feature of the GPS velocity fields of El Salvador, southern Honduras, and Nicaragua is the uniform W- to NW-directed motions of sites in the Central America forearc and corresponding absence of any inland-directed, trench-normal component of station motion anywhere in the forearc or backarc (Fig. 2). The observed velocity pattern differs significantly from the velocity patterns for coastal areas onshore from many other subduction zones, where frictional coupling of the subduction interface causes elastic shortening of the upper plate and landward, approximately trench-normal GPS station motions. GPS sites in the forearc of southern Guatemala also move ~10 mm yr^{-1} to the west relative to stations inland from the volcanic arc (Lyon-Caen et al., 2006), thereby extending the observed pattern of westward forearc translation all the way to the diffuse Cocos–Caribbean–North America triple junction in southern Guatemala.

Modeling of the GPS velocity fields of Guatemala (Lyon-Caen et al., 2006) and Nicaragua (LaFemina et al., 2009) indicates that there is little or no frictional coupling of the subduction interface offshore from either country at depths below 20 km, where earthquakes normally nucleate. Similarly, an inversion of GPS velocities from El Salvador and Nicaragua (Correa-Mora et al., 2009) indicates that interseismic subduction coupling offshore from El Salvador and the northwest half of Nicaragua must be weak or zero (less than 10%) from the trench downdip to depths of 60 km. The absence of measurable trench-normal elastic shortening at onshore sites, and weak implied coupling for much of the subduction interface offshore from Guatemala, El Salvador, and much of Nicaragua, suggest that there may be only limited hazard from large, shallow subduction thrust earthquakes along this part of the Middle America subduction zone.

Trench-Parallel Component of Station Motions

El Salvador

GPS stations in the forearc of El Salvador move toward N70°W-N85°W (Fig. 2A) at rates that increase systematically from ~5 mm yr^{-1} in areas inland from the volcanic arc to ~16 mm yr^{-1} at sites near the Pacific coast (Fig. 2B). The trench-parallel directions of the GPS site motions and difference of 10–15 mm yr^{-1} in the rates of sites on either side of the volcanic arc agree with the abundant seismologic (Fig. 1; White, 1991; White and Harlow, 1993) and geologic (Corti et al., 2005) evidence for right-lateral slip across approximately E-W–trending faults in the volcanic arc.

The S-shaped pattern of the GPS site rates projected onto an arc-normal transect (left panel of Fig. 2B) is similar to rate profiles across other locked strike-slip faults (e.g., Schmalzle et al., 2006). Correa-Mora et al. (2009) used a three-dimensional (3-D) finite-element mesh that approximates the geometries of the Salvadoran volcanic arc faults and the subduction interface (Fig. 4) to estimate the magnitude and distribution of frictional coupling across the volcanic arc faults from GPS station velocities shown in Figure 2. Their best-fitting model indicates that the volcanic arc faults are fully coupled, as expected given the historical and recent record of damaging earthquakes along these faults (White and Harlow, 1993; Martínez-Díaz et al., 2004).

Nicaragua

Stations in the Nicaraguan forearc move toward N50°W-N60°W (upper panel of Fig. 2) at rates of 12–22 mm yr^{-1} (lower right panel of Fig. 2), parallel to the trench offshore. With respect to areas inland from the volcanic arc, sites along the coast of Nicaragua move ~15 mm yr^{-1}, i.e., nearly the same as in El Salvador. The velocities of the Nicaraguan GPS sites are significantly noisier than those from El Salvador, most likely because the Nicaraguan stations have fewer station-days per occupation and shorter time series than for the Salvadoran sites.

TEST FOR MOTION BETWEEN THE SALVADORAN AND NICARAGUAN FOREARCS

The consistency of the fastest slip rates recorded at GPS stations in both the Salvadoran and Nicaraguan forearcs (Fig. 2) suggests that the two forearcs may move as part of the same crustal sliver. We tested this hypothesis in two stages. We first tested whether the two forearcs rotate around a single pole or separate poles via inversions of the azimuths of the GPS station velocities from the two forearcs. We then tested for significant differential rates of motion for the two forearcs. In a companion study, Correa-Mora et al. (2009) estimated frictional coupling across the offshore Middle America subduction interface and faults in the volcanic arc while assuming that the two forearcs move as a single crustal sliver. Here, we test rigorously for relative motion between the forearcs using the same finite-element mesh (Fig. 4) and many of the same procedures, suitably modified and described below.

One- Versus Two-Pole Models for Nicaraguan and Salvadoran Forearc Motions

We tested whether the motions of the two forearcs are better described by one or two poles

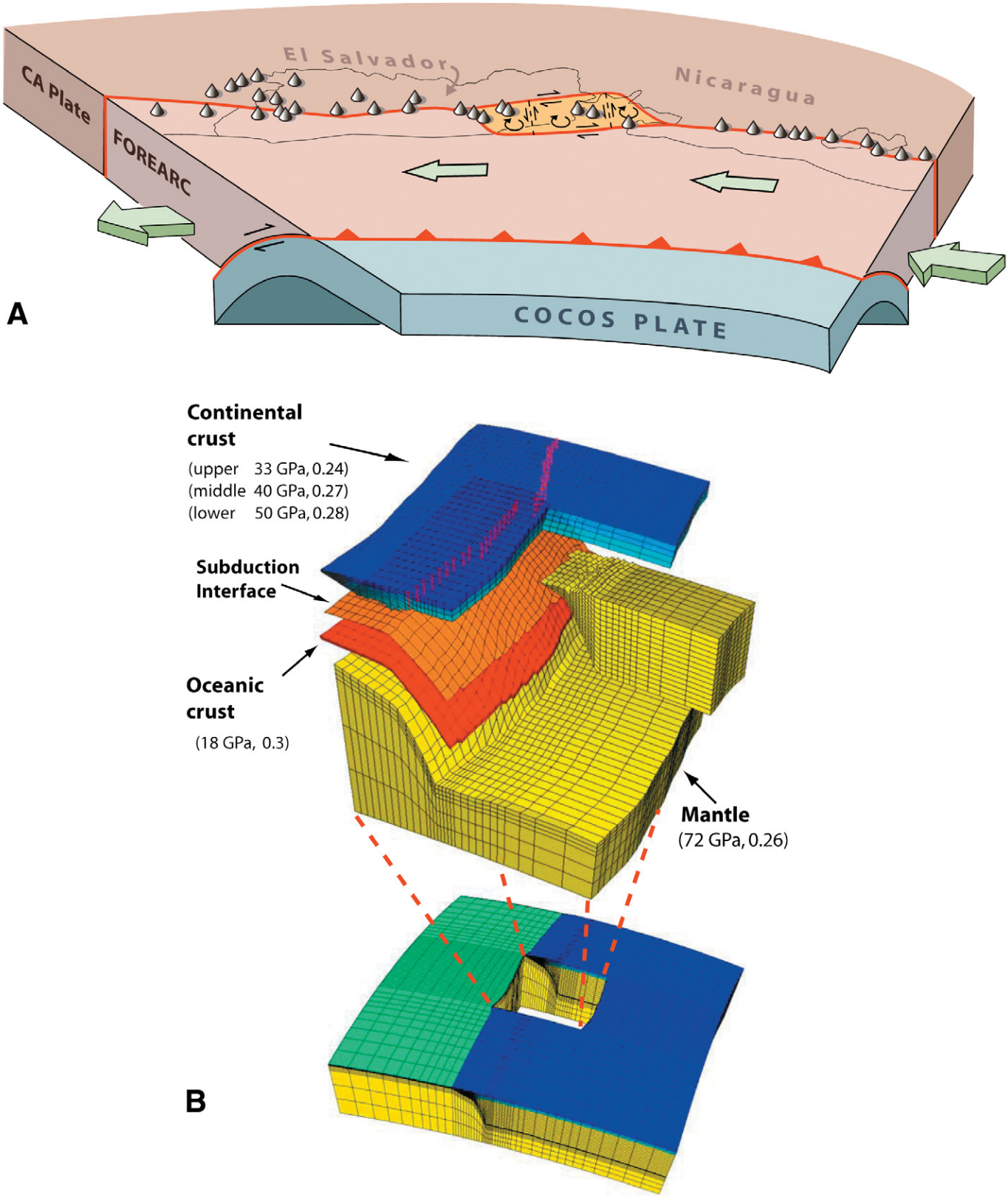

Figure 4. (A) Three-dimensional, schematic illustration of the possible geometry of the forearc-bounding fault and forces that move the Nicaraguan and Salvadoran forearcs. CA—Caribbean. (B) Three-dimensional finite-element mesh used to approximate elastic deformation in the study area. Red dots in the uppermost layer show vertical volcanic arc faults that define the inland edges of the forearc sliver. Dense mesh centered on the study area is embedded in a larger regional mesh to minimize modeling artifacts. The elastic properties assigned to each layer (the shear modulus and Poisson's ratio) are specified within parentheses. Mesh is the same as that used by Correa-Mora et al. (2009).

of rotation by inverting the GPS site velocity azimuths from the two forearcs to find the pole or poles that minimize the weighted least-squares misfit to those azimuths. Eight stations in El Salvador and 13 stations in Nicaragua are located on the forearcs of these two countries. Two of the eight sites in El Salvador, JUCU and SAIN in eastern El Salvador, are located in a region of distributed deformation (see following section) and are thus excluded from this part of the analysis. If both forearcs move as part of a single undeforming block, then the velocity azimuths of the 19 remaining stations on the two forearcs should be well fit by a single pole of rotation. An inversion of the 19 velocity azimuths gives a best-fitting pole of 4.5°N, 91.2°W for the motion of the forearc relative to the Caribbean plate, with an associated least-squares misfit (χ^2) of 25.8. Separate inversions of the six Salvadoran site velocity azimuths and 13 Nicaraguan site velocity azimuths to estimate best-fitting poles for each give a summed χ^2 of 23.1. The improvement in fit for the two-pole model relative to that for the one-pole model, $\Delta\chi^2 = 2.7$, is statistically insignificant ($p = 0.43$) based on an F-ratio test for 2 versus 15 degrees of freedom ($F = 0.9$). The simpler one-pole model thus fits the velocity azimuths adequately and is used herein as the basis for testing whether the trench-parallel rates of motion of the two forearcs differ significantly.

Test for Differential Rates of Forearc Motion

Finite-Element Mesh, Model, and Inversion Method for GPS Velocities

The finite-element mesh we used to estimate the long term rates of motion for the Nicaraguan and Salvadoran forearcs and distribution of interseismic coupling across the subduction interface and volcanic arc faults (lower panel of Fig. 4) approximates the geometry of the subduction interface and volcanic arc faults of El Salvador and Nicaragua and is based on seismic and geologic data described by Correa-Mora et al. (2009). The mesh includes oceanic crust beneath the subduction interface and distinct upper, middle, and lower layers in the continental crust (Fig. 4). Elastic properties for each of these layers were estimated from the seismologically derived CRUST2 model (Bassin et al., 2000). The mesh nodes that represent the volcanic arc faults and subduction interface are spaced closely enough to capture any variations in interseismic coupling across these features revealed by our GPS velocity field. The part of the mesh centered on the study area is embedded within a regional mesh (Fig. 4) that is large enough to minimize any edge effects associated with the mesh. Readers are referred to Correa-Mora et al. (2009) for a description of the mesh boundary conditions and tests used to validate the deformation it predicts.

The horizontal and vertical motions of each GPS site on the surface of the mesh were determined with ABAQUS finite-element modeling software. The motion at each site is a vector sum of the 3-D motions caused by interseismic coupling across the subduction interface, interseismic coupling across faults in the volcanic arc, and assumed long-term motion of the forearc. For the purposes of this study, the interseismic coupling at the nodes that define a fault varies from 0 (for a fault that creeps at its full long-term slip rate) to 1 (for a fault along which elastic strain accumulates at a rate equal to the full long-term slip rate). We computed Green's functions at each GPS site for each mesh node that defines the subduction interface by invoking a unit back-slip velocity at each node to find the resulting 3-D velocity at each site. Green's functions for the nodes that define the volcanic arc faults were determined in two stages. We first imposed a unit coseismic slip rate at each volcanic arc node in order to determine the 3-D elastic response at each GPS site. We then subtracted the coseismic elastic response at each site from an assumed long-term slip rate that was applied uniformly to all of the nodes. This approach gave the desired interseismic Green's function for each node-station pair. A test of this procedure for a long, vertical strike-slip fault gave an interseismic velocity field the same as that produced by analytical solutions (Correa-Mora et al., 2009).

For n GPS sites and m nodes for which we estimated interseismic coupling across the volcanic arc faults and subduction interface, the Green's functions constitute a $3n \times m$ matrix, consisting of three orthogonal Green's functions per GPS site per node. Best estimates for the interseismic coupling coefficient at each node were determined by solving the linear system $Gm = d$, where m is the m-element vector with the coupling coefficients and d is the $3n \times 1$ data vector with the horizontal and vertical components of the GPS site velocities. Best estimates of m for each assumed long-term forearc slip rate were determined using a bounded-variable, least-squares algorithm. Smoothing was applied using a rigorous procedure to identify the smoothing coefficient that optimizes the tradeoff between the smoothed least-squares fit to the GPS velocity field and model simplicity (Correa-Mora et al., 2008). For each inversion, we used a smoothing coefficient of 0.7, which Correa-Mora et al. (2009) identified as the optimal smoothing coefficient. Use of the same smoothing coefficient for all the inversions ensures that any change in the weighted least-squares misfits is attributable only to the different forearc slip rate used for each inversion.

Single Forearc Model

Our test for significantly different rates of trench-parallel motion for the Salvadoran and Nicaraguan forearcs used the velocities of 31 GPS sites from El Salvador, southern Honduras, and Nicaragua that are located close enough to the volcanic arc to record useful information about elastic strain accumulation across faults in the arc. Only two station velocities were excluded, those for sites SAIN and JUCU (Fig. 5), which are located in a region of distributed extensional deformation in southeastern El Salvador. The site velocity uncertainties were taken from Correa-Mora et al. (2009).

For a model in which the Nicaraguan and Salvadoran forearcs are required to rotate around a single pole and move at identical long-term rates, repeated inversions of the 31 site velocities for forearc slip rates from 9 to 19 mm yr^{-1} yielded a best least-squares misfit ($\chi^2 = 254.6$) for a long-term slip rate of 15 ± 1 mm yr^{-1} (1σ uncertainty). Correa-Mora et al. (2009) estimated a best long-term rate of 14 ± 2 mm yr^{-1} but included the velocity for station JUCU, where distributed deformation likely biases the station motion relative to that expected for the forearc. The pattern of velocity misfits is nearly the same as shown in Figure 5b of Correa-Mora et al. (2009), with larger average misfits for stations in Nicaragua (2.5 mm yr^{-1}) than El Salvador (2.1 mm yr^{-1}).

For our revised best-fitting 15 ± 1 mm yr^{-1} forearc slip rate, the optimal interseismic coupling estimates for faults in the volcanic arc and for the Middle America subduction interface are indistinguishable from those determined by Correa-Mora et al. (2009). In both solutions, the volcanic arc faults are strongly coupled nearly everywhere along the arc, and the subduction interface is weakly coupled at all potentially seismogenic depths (0–60 km) and nearly everywhere along strike. Given that none of the interseismic coupling estimates derived for this analysis differs significantly from those described in detail by Correa-Mora et al. (2009), we refer readers to that study for a detailed discussion of interseismic coupling in the study area and focus hereafter only on the long-term forearc slip rates.

Two-Forearc Model

Using the same procedure, we separately inverted the 15 GPS site velocities from El Salvador and 16 Nicaraguan station velocities to find best long-term forearc slip rates for each forearc. The velocities at stations in El Salvador are best fit assuming a long-term forearc slip

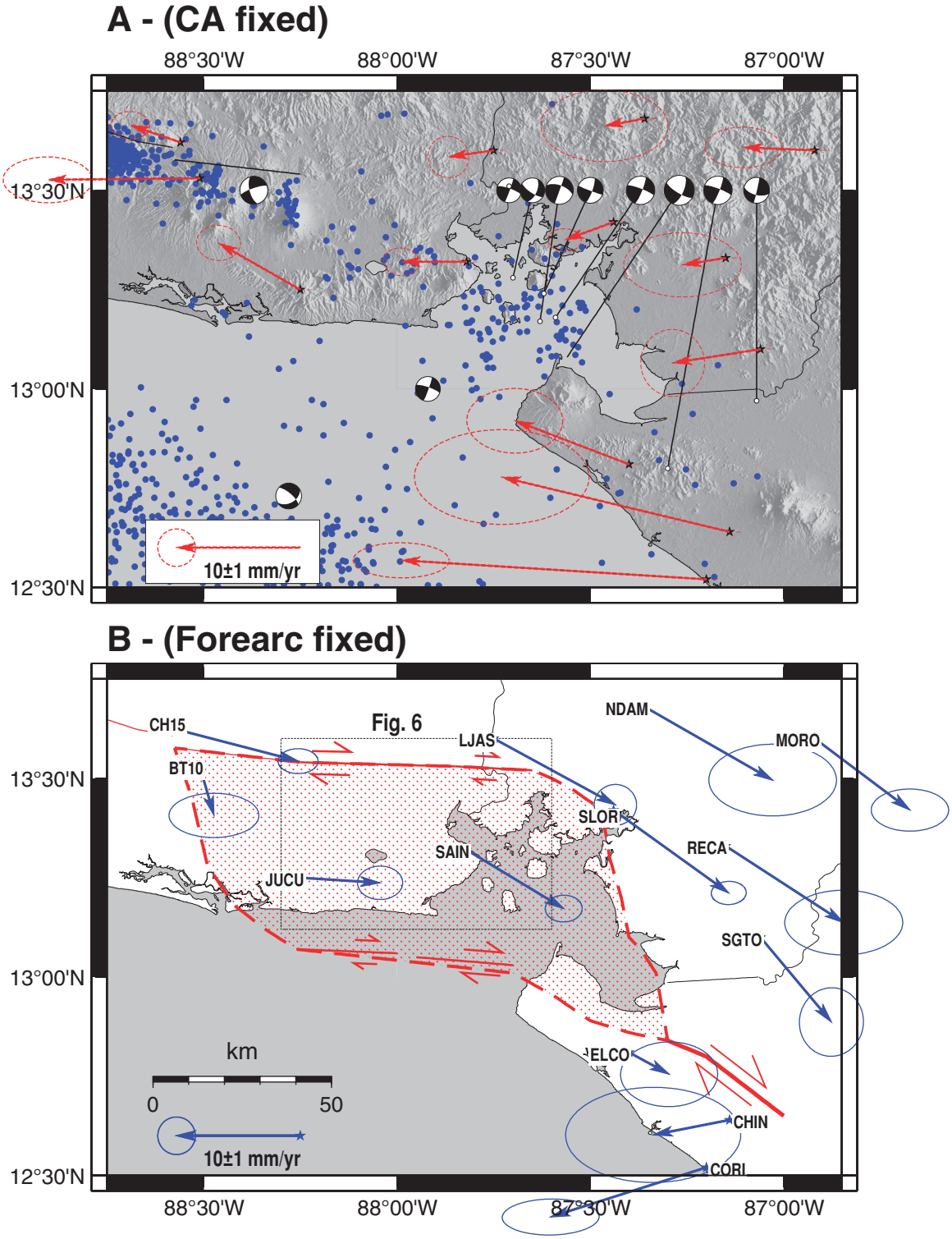

Figure 5. (A) Map of Gulf of Fonseca region with Global Positioning System (GPS) velocities relative to Caribbean plate, shallow-depth earthquake focal mechanisms from the Global Centroid Moment Tensor Catalog and DeMets (2001), and 1984–2010 epicenters for earthquakes shallower than 20 km from the national seismic network of El Salvador (SNET; blue circles). CA—Caribbean. (B) Schematic diagram of Fonseca pull-apart zone (stippled red) and motions of GPS stations relative to the combined Salvadoran and Nicaraguan forearc sliver.

rate of 15 ± 2 mm yr^{-1}, which is modestly slower than the 17 ± 2 mm yr^{-1} slip rate that best fits the Nicaraguan data. The summed least-squares misfit for the two best-fitting models, χ^2 = 243.2, is less than the misfit for the simpler single forearc model (χ^2 = 254.6). The improvement in fit for the two-forearc model relative to that for the one-forearc model, $\Delta\chi^2$ = 11.4, is statistically insignificant (p = 0.06) based on an F-ratio test for 1 versus 79 degrees of freedom (F = 3.66). The average misfit of this more complex model to the Salvadoran station velocities remains nearly the same as for the simpler single forearc model, but it decreases modestly to 2.2 mm yr^{-1} for the Nicaraguan stations. The two-forearc kinematic model is thus rejected.

Kinematic Summary and Implications for the Gulf of Fonseca

GPS station velocities from our study area are consistent with a model in which the Nicaraguan and Salvadoran forearcs move 15 ± 2 mm yr^{-1} (95% confidence limit) as a single crustal sliver parallel to their respective volcanic arcs. Based on the ±1–2 mm yr^{-1} standard errors in our estimates of the individual forearc slip rates, our results indicate that any difference in the trench-parallel movements of the two forearcs is likely to be less than ~3 mm yr^{-1}. The average velocity misfit for the one-forearc model is 1.8 times larger than the estimated velocity uncertainty. The velocity uncertainties may thus be underestimated, or our finite-element model and/or assumption of no deformation within the forearc may be oversimplified.

The trench-parallel motion of the Salvadoran forearc is surprising given that Cocos plate subduction beneath El Salvador is perpendicular to the trench and thus incapable of driving the forearc along the trench. The identical translation rates of the Salvadoran and Nicaraguan forearcs are also unexpected given the ~20°–25° difference in the obliquity of convergence beneath the two forearcs (Fig. 1). This result strongly suggests that the two forearcs are mechanically coupled and also implies that active faulting and seismicity in the Gulf of Fonseca are unlikely to be caused by significant differential motion between the Salvadoran and Nicaraguan forearcs. Next, we use a variety of new structural observations from southeastern El Salvador and the kinematic results described here to better understand deformation across the Gulf of Fonseca.

DEFORMATION IN EASTERN EL SALVADOR AND THE GULF OF FONSECA

In contrast to the narrow, seismically active fault zone in the volcanic arc of central El Salvador (Martínez-Díaz et al., 2004; Corti et al., 2005), earthquakes in the Gulf of Fonseca and eastern El Salvador, where the Salvadoran and Nicaraguan forearcs meet, are diffuse and define a broad deforming zone, with the most intense seismicity focused in the Gulf of Fonseca (Fig. 5). Although these earthquakes might be interpreted as evidence for a collision between the two forearcs, the geodetic evidence described here instead indicates that the two forearcs move together. The many earthquakes in this region are therefore more likely to be a response to the ~40 km right-stepping offset of the volcanic arc combined with the dextral, W to NW motion of the forearc. Deformation across this releasing bend may be accommodated by some combination of distributed normal faulting, bookshelf faulting, or possibly motion along a throughgoing, narrow fault zone accompanied by minor distributed faulting.

Earthquake focal mechanisms offer one source of information about the nature of deformation across the Fonseca offset (Figs. 1 and 5). All focal mechanisms published for earthquakes within or near the Gulf of Fonseca are strike-slip with WNW-ESE– and NNE-SSW–trending nodal planes (Fig. 5). No data are available to determine the fault planes for these earthquakes, leaving unanswered the question of which one of the two nodal planes accommodates slip. Nonetheless, strike-slip faulting driven by right-lateral shear across the volcanic arc clearly contributes to deformation in the Gulf of Fonseca, either via right-lateral strike-slip motion along one or more WNW-striking faults or left-lateral strike-slip bookshelf faulting along NNE-striking faults.

We next describe new geological observations from eastern El Salvador that bear on the nature, timing, and spatial distribution of active faults in this region and possibly the Gulf of Fonseca.

Regional Fault Patterns

Fault traces in southeastern El Salvador were determined using a 10-m-resolution digital elevation model (DEM) of El Salvador. Faults were mapped based on standard methods for aerial photos and DEMs. Our main criterion for identifying a fault was the presence of a linear feature several kilometers or longer that marked a distinct topographic change. Valleys oriented radially outward from volcanic peaks were excluded. The map of faults in eastern El Salvador and the Gulf of Fonseca is shown in Figure 6. In general, faults are dominantly oriented N-S throughout this region and occur most prominently in the mountainous areas. NW-SE– and NE-SW–trending faults also occur locally. Several small lakes in the region occur adjacent to these inferred faults, suggesting graben or half-graben formation. Minor E-W–trending faults are inferred, primarily along the proposed eastward continuation of the El Salvador fault zone. The inferred faults are similar to faults identified by Wiesemann (1975) and Carr and Stoiber (1977) from aerial photographs and field observations.

Our own field reconnaissance indicates that faults in eastern El Salvador consist dominantly of N-striking, normal faults, in accord with our DEM analysis. Normal faults were observed throughout the region in well-exposed, albeit rare, quarries and road cuts. Particularly in Sierra de Jucuaran, an elevated region that parallels the southern coast of El Salvador (Fig. 6), these faults show geomorphic evidence for offset along them. In this area, offsets appear to be predominantly W-side-down on W-dipping faults, indicating the formation of a series of half grabens. Deep tropical soils and dense vegetation in the area did not allow direct observation of most of the large-scale faults. Small-scale faulting is prevalent in this area on most observed outcrops, and the density of faulting increases in proximity to the inferred larger faults. Slickenside striae recorded on these small-scale faults largely indicate dip slip, normal sense motion, but also include oblique slip at high rakes. Normal faulting thus dominates the offset volcanic units we found in this region.

Except for rare subhorizontal slickensides, we found no evidence for strike-slip faulting in eastern El Salvador. In particular, reconnaissance field work targeted on the proposed eastward continuation of the El Salvador fault zone (Martínez-Díaz et al., 2004) revealed no evidence for a major, active strike-slip fault. Martínez-Díaz et al. (2004) proposed that this fault exists based on a topographic lineament that follows the trend of the El Salvador fault zone eastward (Fig. 6) and the occurrence of a right-lateral offset of the San Miguel River across this lineament. Although we found the trace of a major, E-W–striking fault near the San Miguel River, just north of the town of San Miguel, we found no compelling geomorphic evidence for an eastward continuation of this fault along strike in the DEM or in the field. For example, volcanic units adjacent to the Gascoarán River, locally the boundary between El Salvador and Honduras, showed minimal fracture development along the trend of the proposed eastward continuation of the El Salvador fault zone. The subdued and seemingly discontinuous topographic expression of the proposed fault in this region (Fig. 6) and lack of associated fracturing along the proposed trend of the El Salvador fault zone in eastern El

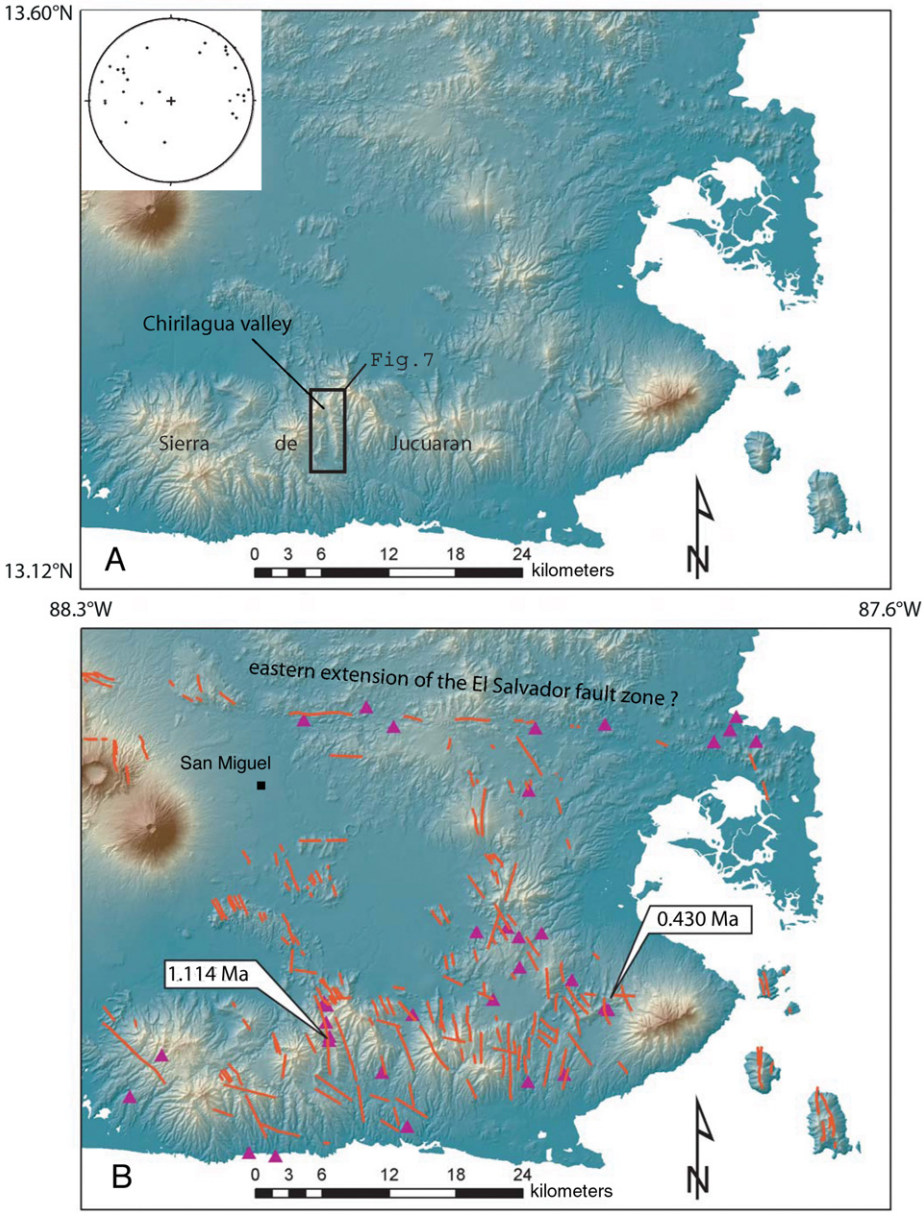

Figure 6. (A) 10 m digital elevation model (DEM) of eastern El Salvador showing location of Figure 7. (B) Faults interpreted from the DEM (red lines), field evaluation stations (purple triangles), locations and $^{40}Ar/^{39}Ar$ dates of two samples (white flags), and equal-area stereonet plots showing poles to fault planes measured during field evaluation (inset on left side).

Salvador suggest that forearc motion is partially accommodated by other structures.

Age of Faulting

The age of faulting in the study area is constrained by the age of volcanic units that are cut by the numerous normal faults. We dated two volcanic units with $^{40}Ar/^{39}Ar$ analysis done at the Rare Gas Geochronology Laboratory at the University of Wisconsin. Details of the age dating are given in Table 1 and in Alvarado (2008). The first sampling locality occurs on a well-exposed normal fault in Sierra de Jucuaran, herein named the Chirilagua fault. This fault is described in detail in the following section (location is shown in Fig. 7 and given in footnotes to Table 1). The sample is from a basaltic lava flow taken within 20 m of the top of the footwall (east side) of the W-dipping normal fault and thus represents one of the youngest bedrock units affected by the Chirilagua normal fault. The $^{40}Ar/^{39}Ar$ radiometric analysis gives a preferred age of 1114 ± 40 ka for this volcanic unit (Table 1). Our second sample is from an andesitic pumice tuff exposed in a rock quarry on the west side of the Conchagua volcano, near the Gulf of Fonseca (Fig. 6). This volcanic unit is offset by 33 cm by several normal N-striking normal faults. This unit is assumed to be relatively young given the less fractured nature of the outcrop (which may be partially a function of the unlithified nature of the outcrop) and the lack of abundance of fractures relative to other outcrops in eastern El Salvador. This sample has a best $^{40}Ar/^{39}Ar$ age date of 430 ± 72 ka (Table 1).

The age of the two volcanic units indicates that normal faulting in eastern El Salvador is younger than 430 ka. These data are consistent with field observations of normal faults that cut upward to the surface. The Chirilagua fault is one of the normal faults recognized on the DEM, while the second site has only distributed small-scale faulting. The young ages for both units indicate that both the large-offset and small-offset faults are recent, and that the area is currently experiencing distributed, extensional deformation over a large region.

Chirilagua Fault

Despite the abundance of normal faults in eastern El Salvador, there are relatively few good outcrops of the larger-offset faults due to cover by dense vegetation. One such fault, herein named the Chirilagua fault due to its proximity to the town of Chirilagua, is subparallel to a major north-south road (CA-2) (Fig. 7) and is superbly exposed in road cuts along this road. There are three main exposures of the fault. The two southern fault outcrops are ~30 m high and ~50–60 m wide and provide fresh exposures (Fig. 8). The northern fault outcrop consists of a recently exposed fault plane that is ~5 m high and ~20 m wide, upslope from which a deeply weathered fault surface extends another 3–4 m. We assume that the newly exposed fault surface was exhumed during the construction of the adjacent road. The effect of construction appears to have been minimal, with excavation scars easily identified as short (1–2 m), curvilinear, subhorizontal scratches that were likely produced by a backhoe.

The Chirilagua fault has an average orientation of 194° and dips steeply (80°) to the west. The footwall rocks of the fault consist of a series of basalt flows. The hanging-wall rocks, where not exhumed by road construction, consist mainly of highly fractured basalt and soil (Fig. 8). Asymmetric chatter marks (e.g., Doblas, 1998) on the fault surface indicate W-side-down motion. The direction of fault slip is indicated by the orientations of tool marks and slickenlines exposed on the fault surface (Fig. 9A). Slickenline orientations measured by hand show three main clusters: (1) downdip (~45%

TABLE 1. SUMMARY OF $^{40}Ar/^{39}Ar$ EXPERIMENTS

Sample	Experiment	Material	Total fusion age (ka ±2σ)	K/Ca total	Weighted mean analysis			N	Isochron analysis		
					^{39}Ar %	MSWD	Age (ka ±2σ)		$^{40}Ar/^{39}Ar$ (±2σ)	MSWD	Age (ka ±2σ)
07SJ-17	UW68B18	Plagioclase	439.1 ± 46.9	0.020	100.0	0.84	430.4 ± 72.1	12 of 12	295.4 ± 4.5	0.92	430.4 ± 72.1
07SJ-2	UW68B16	Groundmass	1085.9 ± 44.5	0.117	86.7	0.80	1113.7 ± 40.1	7 of 9	285.2 ± 25.2	0.85	1318.7 ± 459.9

Note: All ages were calculated using the decay constants of Steiger and Jäger (1977; $\lambda_{40K} = 5.543 \times 10^{-10}$ yr^{-1}). Ages are relative to 28.02 Ma Fish Canyon sanidine (Renne et al., 1998). Ages in bold are preferred. Coordinates of samples 07SJ-17 and 07SJ-2 are 13°15.5′N, 88°7.45′W and 13°17.0′N, 88°7.45′W, respectively. MSWD—mean square of weighted deviates.

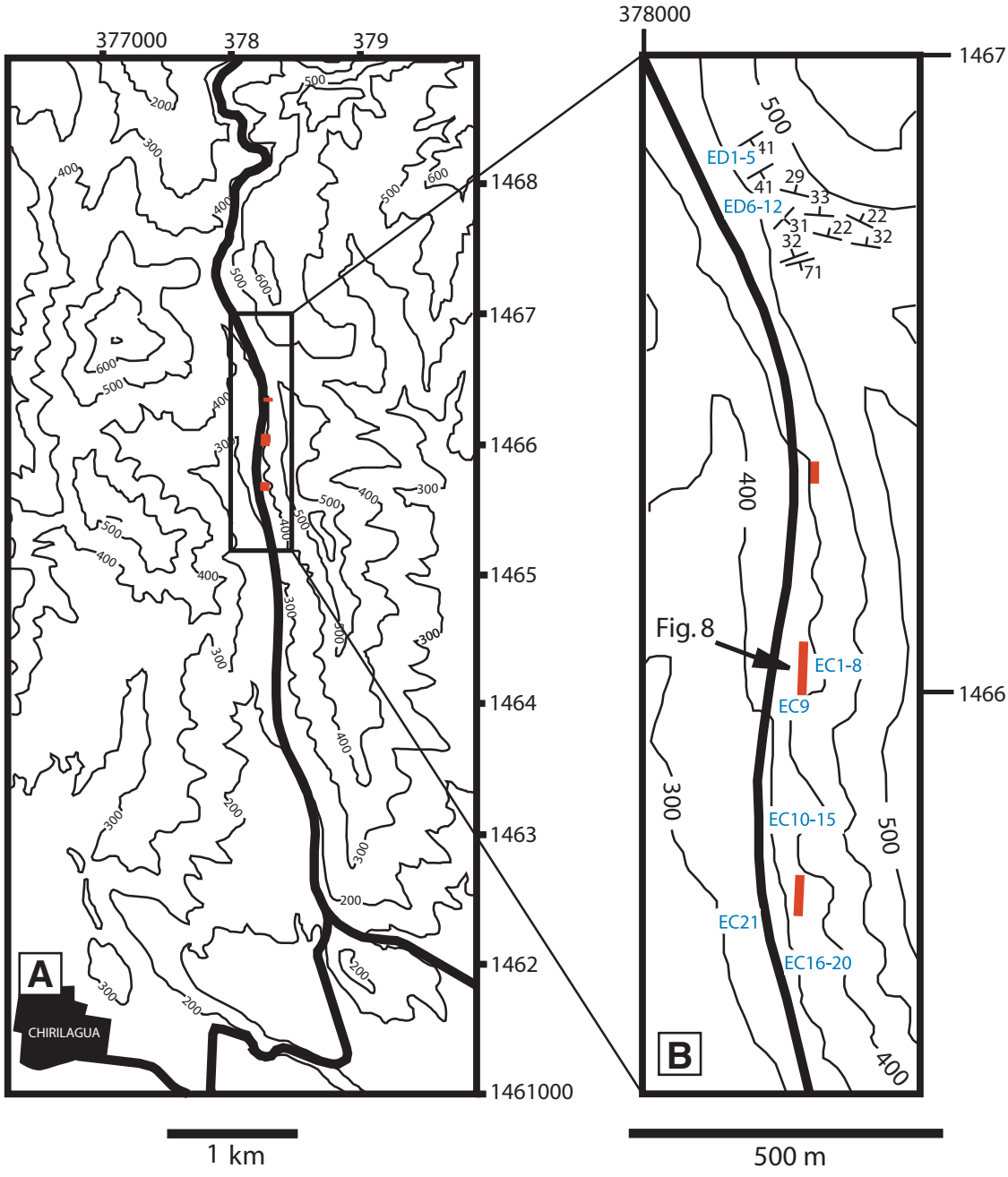

Figure 7. (A) Line drawing of Chirilagua Valley topography with 100 m contour intervals. Thick black line and solid black polygon represent Highway CA-2 and the town of Chirilagua, respectively. Black rectangle represents location of B. Short red lines show Chirilagua fault outcrops. Coordinates are in UTM projection. (B) Locations of the three outcrops of the Chirilagua fault (red lines), paleomagnetic stations (blue), strikes and dips of lava flows for stations ED3–12 (black lines), and location of Figure 8 superimposed on 50 m elevation contours.

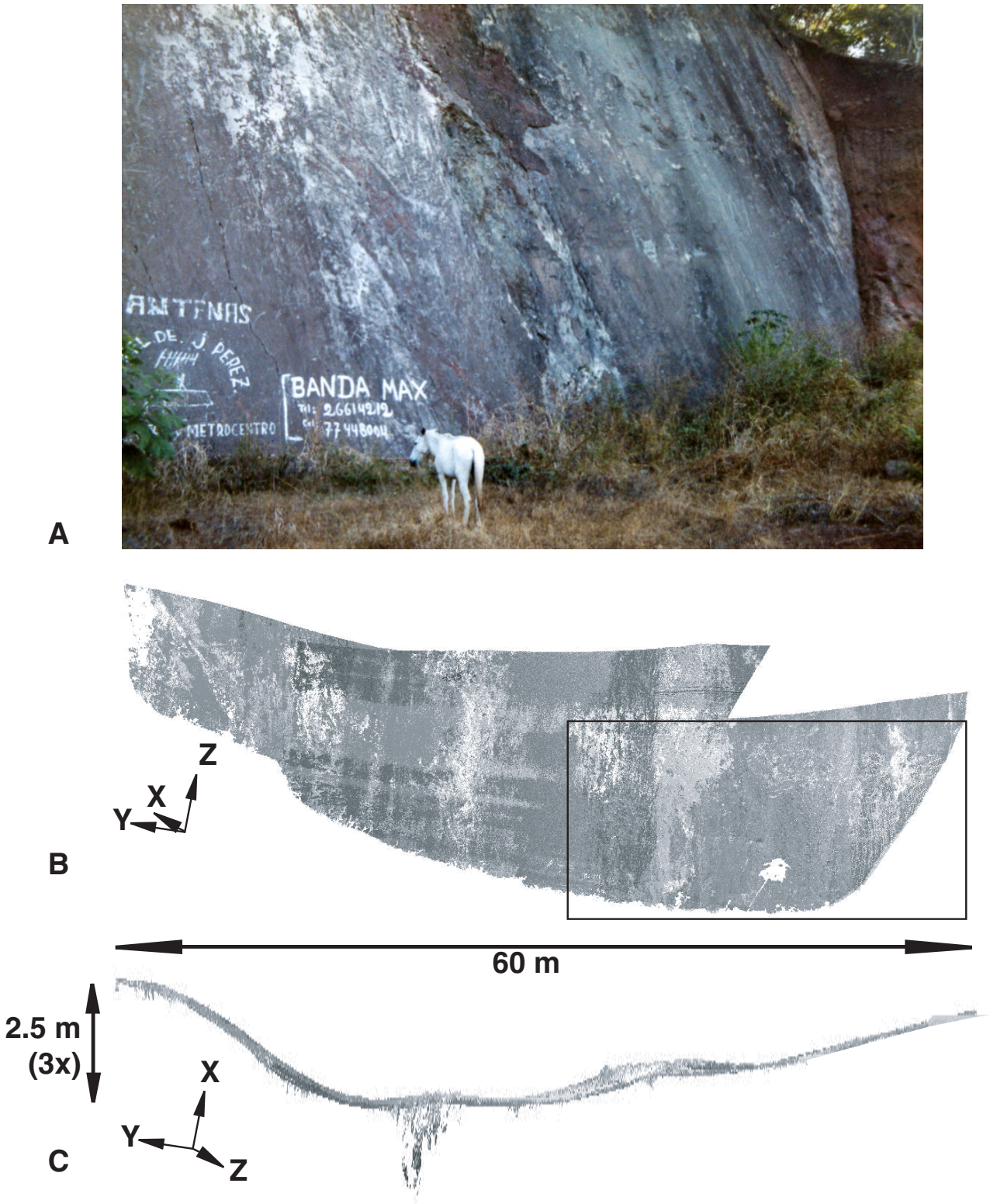

Figure 8. (A) Photograph of southern portion of central outcrop of the Chirilagua fault. (B) Lidar reflectivity image of part of the fault surface shown above. The Terrestrial Lidar Scanner generates a scan of the target producing (*x, y, z*) positional data for each laser pulse that strikes the scan area, producing a point cloud for digital display. The system records the reflectivity for each pulse, represented as a gray scale value in this image. The black rectangle shows the part of the fault surface shown in the above photograph. Lighter-colored objects tend to have stronger reflectivity. (C) Looking down on the image in B, with an applied exaggeration perpendicular to the fault surface. This view illustrates large-scale irregular corrugation of the fault surface, where the corrugation represents the long-term slip direction for the fault. Oblique lineations observed in the field (Fig. 10) and within the Lidar intensity data above indicate a late, strike-slip overprint.

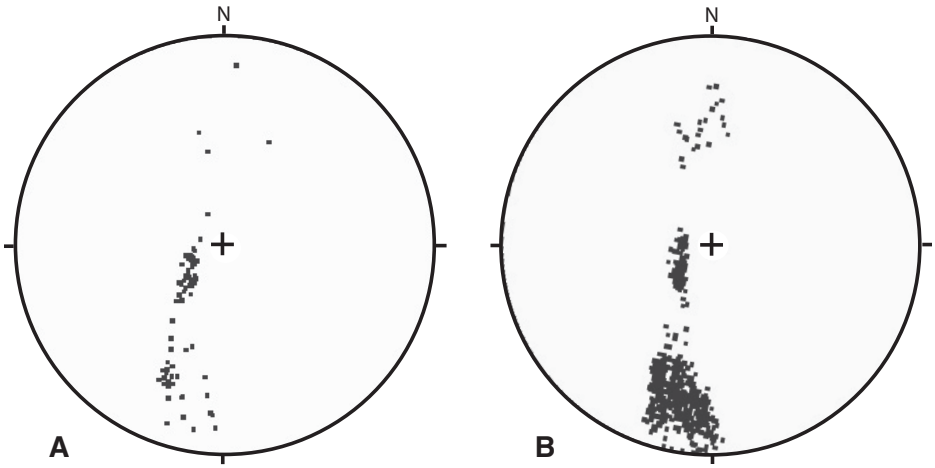

Figure 9. Stereonet plot of fault striae measured in the field (A) and on the Terrestrial Lidar Scanner model (B).

of the measurements); (2) moderately S pitching (~45% of the measurements); and (3) moderately N pitching (~10% of the measurements). Taken together, the field observations indicate that the Chirilagua fault is dominantly a normal fault, but it may have also accommodated right-lateral oblique slip, corresponding to the N-pitching lineations, followed by left-lateral oblique slip, corresponding to the S-pitching lineations. Crosscutting relationships between the different tool marks indicate that the S-pitching lineations occurred after the formation of the downdip lineations (Fig. 10). We interpret this pattern to indicate that downdip slip was followed by a phase of left-lateral oblique slip.

The fault surface also contains several 20-m-wavelength corrugations that have peak-to-trough amplitudes of 1–2.5 m, characterized using Lidar (see following). As a result, the fault strike varies from 178° to 204°. Fault gouge is preserved in the corrugation troughs but is absent from the corrugation ridges. The fault corrugation ridges are also polished on their NW-facing surfaces, whereas on their SW-facing surfaces, tool marks filled with gouge remain well preserved. This pattern indicates that sinistral offsets may have occurred late in the slip evolution of this fault.

Figure 10. Photograph of crosscutting relationships between downdip and left-lateral oblique kinematic indicators observed at the Chirilagua fault.

Terrestrial Lidar Scanning

Given the large exposure and complex surface geometry of the Chirilagua fault, we used Terrestrial Lidar Scanner (TLS) to produce a three-dimensional image of the fault surface over the 60 m of continuous exposure. TLS gathers a three-dimensional survey of the fault surface morphology and its laser reflectivity. The 3-D image was produced by an Optech Inc., Ilris 3D 1500 nm, tripod-mounted laser system. Four parameters were recorded for each imaged point on the fault surface: *X*, *Y*, *Z* coordinates relative to an origin at the tripod and a value of reflectivity. A point spacing of 3–35 mm was achieved from a single scan of the fault surface. Point density in the model was increased by recording several scans of the fault surface and manually merging them using Polyworks 10.12 software from Innovmetric. Fault-slip directions can be derived by mapping kinematic markers that are visible on a geospatially referenced 3-D Lidar model. Kinematic indicators such as tool marks and slickenlines produce visible linear anomalies in the reflectivity of the model surface, the orientations of which can be measured with the Lidar, and imaged with the IMView software.

The first-order features that show up in our 3-D Lidar model of the Chirilagua fault are the 20-m-wavelength, 1–2.5-m-amplitude fault corrugations with axes that point downdip (Fig. 8). Linear reflectivity anomalies are also clearly visible (Fig. 8), which occur at smaller (decimeter to meter) spatial scales than the corrugations, and define three distinct clusters. The dominant cluster, constituting ~75% of the lineations we identified, pitches shallowly to the south at ~30° (Fig. 9B). A secondary cluster pitches steeply to the south at ~70° (Fig. 9B) and constitutes ~20% of the lineations we identified. Finally, a minor cluster of lineations pitches to the north at ~30° (Fig. 9B).

Two main conclusions result from our interpretation of the Lidar image. First, the lineations we identified from the reflectivity anomalies (Fig. 9B) correspond well to those that we measured in the field (Fig. 9A). The lineations mapped with the Lidar occur everywhere on the fault surface and thus validate our field measurements, which were limited to the lower

2–3 m of the outcrop that were accessible from the ground. Second, the corrugations occur parallel to the downdip lineations, indicating that the normal motion occurred first and was of greater magnitude than the later left-lateral oblique motion. Thus, the Lidar data help to constrain both the timing and relative magnitude of the fault movement.

Fault Interpretation

The Chirilagua fault is unusual in two respects. First, its ~80° dip is steeper than that of most normal faults. Second, multiple lineation orientations are exposed on the fault surface. We next discuss each of these features.

We hypothesize that the steep dip of the Chirilagua fault represents its original dip. Faults can achieve such dips when blind normal faults propagate upward and/or when they exploit subvertical cooling fractures, as has been documented for normal faults in basaltic rocks in Iceland, East Africa, and Hawaii (e.g., Muffler et al., 1994; Angelier et al., 1997; Peacock and Parfitt, 2002; Grant and Kattenhorn, 2004; Martel and Langley, 2006; White and Crider, 2006). Our hypothesis is supported by the observation that lava flows dip 14° to the east in the footwall of the fault (see paleomagnetic section), indicating that the 80°W-dipping fault was subperpendicular to the lava flows. If the Chirilagua fault is one of a series of half grabens that occur in the Sierra Jucuran, progressive extension in the region would serve to increase the dips of lava flows cut by those faults and decrease the dip of normal faults cutting those flows, in accord with the dips reported here for the Chirilagua fault and the flows cut by the fault.

The number of lineations on the Chirilagua fault is also unusual for a fault surface. As noted previously, the well-developed 20-m-scale corrugations imaged by the Lidar data indicate that the early movement was downdip and this was the direction of maximum displacement. Overprinting of the downdip lineations by the left-lateral oblique lineations (Fig. 10) suggests that the early phase of dip-slip movement was followed by a phase of left-lateral oblique slip. This relationship is also consistent with the spatial relationship between fault gouge and corrugations; the downdip corrugations and gouge between those corrugations were created during an initial phase of downdip slip, after which left-lateral oblique slip polished the gouge off the NW faces of the corrugation ridges and preserved it in the SW faces of the corrugation valleys.

The small population of shallowly N-pitching lineations is more difficult to interpret. The N-pitching lineations did not obviously overprint either of the earlier lineation sets, so the relative timing of this slip phase is unknown. If the N-pitching lineations record a component of normal faulting, then they record a different phase of right-lateral, oblique-slip motion. Alternatively, the N-pitching lineations may represent an early phase of deformation, possibly recorded during propagation of the fault following the model of Kaven and Martel (2007). In such a model, en echelon fractures that are created early in the development of a fault eventually link with each other and with the fault as the fault matures, which results in the development of an irregular fault trace. Changes in stress directions result in changes in slip direction on these preexisting fractures as the fault propagates laterally and breaches Earth's surface (Kaven and Martel, 2007). These types of irregularities are smoothed into outcrop-scale fault corrugations as the fault matures (Ferrill et al., 1999). The large corrugations on the Chirilagua fault are consistent with this interpretation.

Paleomagnetic Analysis

Paleomagnetic data were used to test whether the crustal blocks adjacent to the Chirilagua fault have rotated about vertical and/or horizontal axes. In total, 322 oriented samples were collected with a portable gas-powered drill from 33 sites along ~0.5-km-long transects separated by ~1 km and positioned within the footwall of the Chirilagua fault (Fig. 7). The southern transect (labeled EC in Fig. 7) consists of 21 sites that sample the surface of the Chirilagua fault and the footwall rocks exposed in the central outcrop (sites EC1–8) and a complex of volcanic flows, breccias, and dikes (sites EC9–21). This transect was also the site of our Lidar study and the 1114 ± 40 ka sample dated via $^{40}Ar/^{39}Ar$ analysis. The northern transect (sites ED 1–12) was taken at distance from the fault surface in the footwall block of the Chirilagua fault and consists of 12 sites that sample a sequence of generally E-dipping lava flows.

Methods

Demagnetization of all our paleomagnetic samples was done using alternating field (AF) and thermal treatment at the University of New Mexico paleomagnetism laboratory. All sites received AF demagnetization treatment using a 2G Enterprises Model 760R three-axis superconducting rock magnetometer and its AF demagnetization system in a magnetically shielded room. At least one sample per site received a sequence of fine demagnetization steps of 2 mT up to 20 mT and 5 mT up to 120 or 130 mT. The rest of the samples were typically demagnetized in 10 mT steps up to 120 or 130 mT. Fifty representative samples from all 33 stations were thermally demagnetized using a Schondstedt TSD-1 furnace following the temperature sequence specified in Figure 11.

Sample demagnetization results were plotted on orthogonal demagnetization plots, examples of which are shown in Figure 11. Sample means were calculated with Paleomag 3.1 software (Jones, 2002) through a Fisher least squares regression of selected demagnetization points that included the plot origin to define a best-fitting linear segment. Sample means with maximum angular deviation values greater than 15° were discarded from the initial site mean calculation. Site means and uncertainties were iteratively calculated after discarding samples for which means were more than two angular distances away from the site or transect mean. Orthogonal demagnetization plots show that the response to progressive demagnetization of most samples was linear (Fig. 11). Sample means typically had low mean angular deviation values, with the exception of most sites drilled on the surface of the Chirilagua fault (EC1–8). Most samples showed weak viscous remanent magnetizations that overprint a primary signal believed to represent thermal remanent magnetizations—the viscous component was removed at low fields (10–20 mT) or low unblocking temperatures (below 300 °C). AF treatment with up to 120–130 mT achieved 80% demagnetizations for ~60% of the samples. Further demagnetization using thermal treatment showed no change in magnetic orientation. Thermal treatment with maximum temperatures of 590 °C resulted in more than 99% demagnetization for all samples. A relatively small demagnetization step occurred for most samples at temperatures of 300–350 °C, and most demagnetization occurred at temperatures of 500–590 °C. Curie temperatures and hysteresis loop parameters determined from representative samples are consistent with low-Ti to moderate-Ti magnetite as the dominant magnetic carrier (Alvarado, 2008).

Results

Site means, statistics, and other information are shown in Table 2. Samples from the northern transect (ED) have a tightly clustered mean declination and inclination of 184.0° and –18.9°, respectively, and a Fisher 95% angular uncertainty α_{95} of 6.4° (Fig. 12). Individual sites have low standard deviations, and individual samples have low mean angular deviation values. The southern transect was subdivided into two groups, the means and dispersions of which differ substantially. Sites EC1–8 have a mean of 182.9°, 5.7°, but large scatter of ±30° (95% confidence level). Individual sites in this group have high standard deviations, and individual samples show variable results, with some having

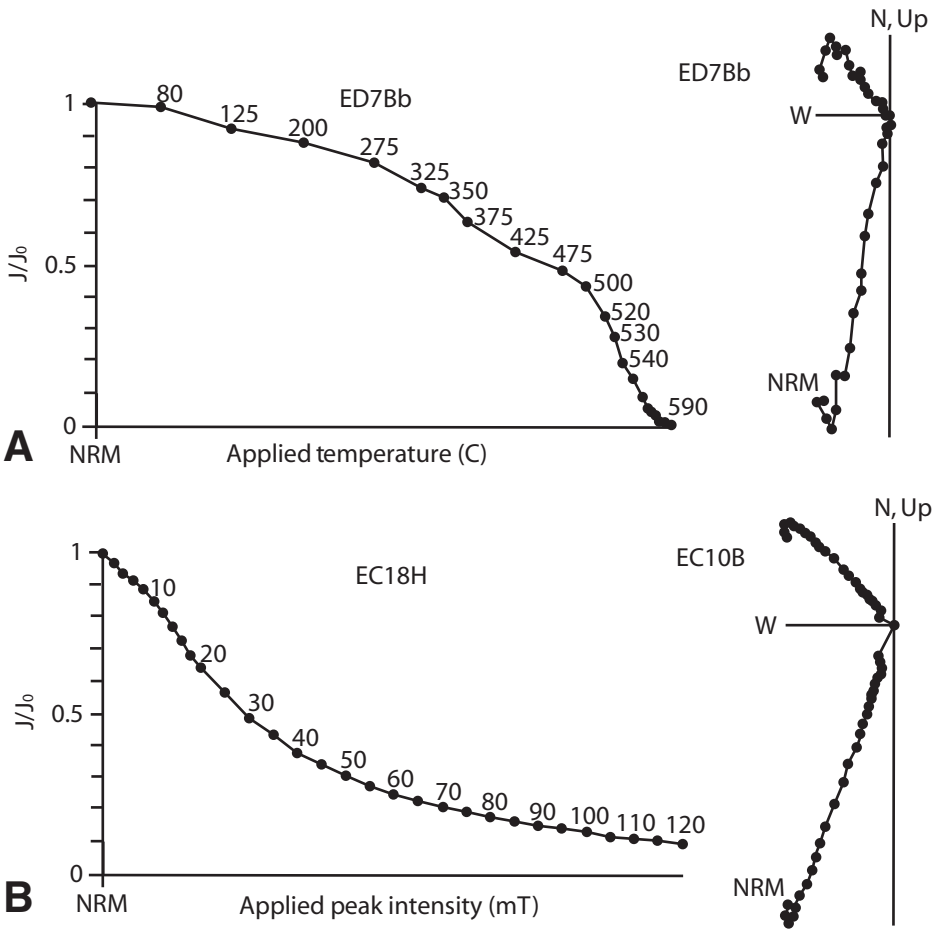

Figure 11. (A) Normalized intensity J/J_o of magnetization versus temperature (upper) and applied alternating field (lower) of representative paleomagnetic samples. (B) Orthogonal diagrams showing magnetic inclination and declination of representative paleomagnetic samples as a function of demagnetization. NRM—Natural Remanent Magnetism.

medium to high maximum angular deviations and most showing large magnetic overprints. Results from sites EC1–8 are excluded from further analysis for this study. The other cluster of sites (EC9–21) from the southern transect have a mean paleopole of 192.0°, –13.0° and 95% confidence limit (±11.8°) nearly a factor of three smaller than for sites EC1–8 (Fig. 12). Individual sites and samples from this group have low to medium standard deviations and maximum angular deviations, respectively.

A stratigraphic correction to the site means was performed to restore the mean orientation of lava flows to a presumably original horizontal attitude. Lava flows sampled on sites from the northern traverse (ED3–11) have a mean strike of 347° and mean dip of 14° to the east. This tilting is presumably due to normal movement along the Chirilagua fault, which rotates the lava flows about a horizontal axis due to slip along a listric fault or by domino-style faulting. If restoration of the lava flows to the horizontal corrects for the downdip component of faulting, the resulting correction should isolate the vertical axis-rotation component.

Stereonet plots of tilt-corrected sites are shown in Figure 12. Correcting the results for sites along the northern transect (ED1–12) by the tilt rotates the declination clockwise by 3.9° and the inclination 4.5° toward the horizontal, yielding a stratigraphically corrected mean declination and inclination of 187.9°, –14.4° (±6.4°). Correcting the results for sites EC9–21 by the tilt rotates the declination clockwise by 2.2° and the inclination 6.2° toward the horizontal, yielding a stratigraphally corrected mean declination and inclination of 194.2°, –6.8° (±11.8°). Combining the results for both of these transects yields a stratigraphically corrected traverse mean direction of 191.2°, –10.6° (±6.7°, 95%).

The expected declination and inclination for young rocks in this location based on an assumption of an axial geocentric dipole are 180° and –25.2° (Butler, 1992). Relative to the expected declination and inclination, our stratigraphically corrected mean direction of 191.2°, –10.6° therefore implies that the footwall rocks have rotated 11.2° ± 6.7° clockwise around a vertical axis and 14.6° toward the horizontal around a horizontal axis since they were extruded onto the surface. Whether or not these are representative of the regional-scale deformation is unknown since our paleomagnetic samples are limited to a single fault-bounded block and may not fully sample secular variation of the paleomagnetic field.

There are two important implications of the paleomagnetic results: (1) the rate of rotation; and (2) the sense of rotation. The clockwise rotation of 11° ± 7°, although small, is detectible using paleomagnetic methods at a 95% confidence level. The rate of rotation, assuming vertical-axis rotation, would be ~26°/m.y. (within a range 7°–42°/m.y., representing the values of the error brackets on the rotation). This rate is quite high because of the relatively young rocks (430 Ma) involved in the deformation. For comparison, rotation rates in the Transverse Ranges of southern California along the San Andreas fault system are typically ~6°/m.y., although rates are locally ~13°/m.y. (Luyendyk, 1991). Perhaps more relevant, paleomagnetically determined, vertical-axis rotation in a pull-apart structure in western Nevada indicates ~25° of clockwise rotation from internal blocks (Petronis et al., 2002), although a rate is difficult to calculate because of ambiguities in the age of magnetic acquisition. The sense of rotation in the El Salvador study area is clockwise, which is consistent with overall dextral shear. Some caution is warranted. In studies with more sampling localities, individual block domains can be distinguished where some domains rotate in a clockwise sense and others in a counterclockwise sense (e.g., Petronis et al., 2002; Avşar, and Isseven, 2009). The lack of exposure in El Salvador did not allow us to sample more broadly, and thus we did not pursue this strategy. Wawrzyniec et al. (2002) argued that there is no straightforward relationship between the sense of shear and the expected rotation of fault-bounded blocks within a broad zone of transcurrent shear. Rather, initial orientation of inherited structures and their obliquity to the primary trend of the deforming zone have primary control in determining if a fault-bounded block will rotate clockwise or counterclockwise in response to transcurrent shear, a result consistent with analog physical models (Markley and Tikoff, 2002). The poor exposure in southeastern El Salvador makes knowing the block geometry difficult, although the main fault trend in the Sierra de Jucuaran is N-S oriented, and

TABLE 2. PALEOMAGNETIC ANALYSIS BY SITE

Site	Lithology	Latitude (°N)	Longitude (°W)	UTM(16) N	UTM(16) W	*n*/*N*	D (°)	I (°)	α_{95} (°)	Bedding
EC1	Fault	13.2595	88.1241	1466107	378221.9	6/10	204.9	10.9	29.4	
EC2	Fault	13.2594	88.1241	1466096	378221.8	5/8	176.9	2.2	27.9	
EC3	Fault	13.2593	88.1241	1466085	378221.8	6/7	170.7	3.3	26.2	
EC4	Fault	13.2593	88.1241	1466085	378221.8	8/11	281.3	–2.5	56	
EC5	Fault	13.2592	88.1241	1466019	378217.2	6/7	164.4	–10.5	9.9	
EC6	Fault	13.2591	88.1241	1466063	378221.7	8/12	182	15.4	34.2	
EC7	Fault	13.2590	88.1241	1466052	378221.6	5/12	176	13.7	33.6	
EC8	Fault	13.2589	88.1241	1466041	378221.6	11/13	145.5	3.5	88.4	
EC9	Breccia	13.2585	88.1240	1465997	378232.2	8/8	165.9	–21.7	12.4	
EC10	Flow	13.2572	88.1240	1465848	378235.9	6/7	180.5	–16.1	3.7	
EC11	Flow	13.2566	88.1238	1465792	378251.3	6/10	183.6	0.6	12.2	
EC12	Dike	13.256	88.1237	1465718	378265.7	11/12	179.5	–17.1	3.3	
EC13	Dike	13.2557	88.1236	1465682	378276.3	4/10	212.3	–29.9	13.8	
EC14	Breccia	13.2556	88.1236	1465676	378279.5	3/4	198.9	–21.2	50.2	
EC15	Dike	13.2554	88.1236	1465676	378279.5	11/13	181.5	–14.4	4.6	
EC16	Flow	13.2551	88.1236	1465620	378273.9	7/8	232.4	–24.9	18.6	
EC17	Flow	13.2550	88.1236	1465609	378273.8	7/12	201.9	8.2	15.9	
EC18	Breccia	13.2548	88.1236	1465587	378278.1	7/12	200.5	–0.9	6.4	
EC19	Flow	13.2547	88.1235	1465580	378284.5	7/8	202.7	–4.1	7.6	
EC20	Flow	13.2541	88.1233	1465498	378237.5	8/9	194.7	8.6	2.1	
EC21	Dike/breccia	13.2552	88.1236	1465627	378270.7	15/19	163.5	–28.2	5.5	
ED1	Flow	13.2660	88.1244	1466826	378192.7	6/7	178.2	–20.6	6.7	
ED2	Flow	13.2655	88.1244	1466772	378192.4	8/10	184.7	–32.4	3.1	
ED3	Flow	13.2655	88.1266	1466772	377954	9/11	182.6	–37.5	3.6	58, 41
ED4	Flow	13.2654	88.1242	1466762	378206.4	7/7	185.3	–20.8	2.3	59, 41
ED5	Flow	13.2653	88.1241	1466747	378222.6	12/14	181.8	–20.5	8.7	60, 41
ED6	Flow	13.2653	88.1240	1466749	378235.6	6/9	187.8	–18.9	2.5	284, 29
ED7	Flow	13.2651	88.1239	1466726	378246.3	7/8	188.4	–12.4	6	274, 33
ED8	Flow	13.2650	88.1239	1466715	378246.3	8/9	182.8	1.3	3	296, 22
ED9	Flow	13.2648	88.1239	1466688	378251.6	7/10	178.5	–30.2	11	43, 31
ED10	Flow	13.2646	88.1238	1466671	378256.9	6/8	185.3	–21.6	4.4	284, 22
ED11	Flow	13.2645	88.1238	1466660	378256.9	7/10	185.5	–9.5	6.6	279, 32
ED12	Flow	13.2644	88.1238	1466650	378253.6	7/7	185.7	–3.7	2.4	250, 32; 76, 71

Note: Columns 1 to 6 specify the paleomagnetic sample codes, sample coordinates, and Universal Transverse Mercator (UTM) coordinates in meters; "*n*" and "*N*" are the number of samples used to find the mean and the number of samples collected at the site, respectively. Paleomagnetic declination (D) and inclination (I) are measured in degrees clockwise from north and degrees down from horizontal, respectively. α_{95} is the Fisherian 95% confidence limit in degrees. Final column gives the strike and dip of the bedding if it could be determined.

the faults are closely spaced (~3–5 km). Thus, we anticipate that the fault blocks are N-S and elongate, although it is unlikely that they extend from the coast inland to the eastern extension of the El Salvador fault zone as coherent blocks. Regardless, N-S elongate blocks oriented at a high angle to an E-W plate boundary in a right-lateral setting are expected to rotate clockwise, consistent with the sense of rotation.

Structural Summary

North-south–oriented normal faults are found throughout eastern El Salvador, suggesting that they accommodate regional extension dominated by E-W elongation. Faulting is recent, because faults cut up to the ground surface through soil layers and locally through two volcanic units with young ages (1114 ± 40 ka and 430 ± 72 ka). Our paleomagnetic analysis indicates that the N-S, elongate fault blocks may have experienced minor clockwise, vertical-axis rotation in the last ~1 m.y. Despite the limitation of the paleomagnetic data to a single site, the observed clockwise rotation is consistent with distributed right-lateral shear (wrench) parallel to the plate margin.

Detailed kinematic analysis from the well-exposed Chirilagua fault shows that it records predominantly downdip, normal movement and most likely formed at a steep dip, presumably by exploiting subvertical cooling fractures in the volcanic units that it offsets. Some amount of later phase left-lateral oblique slip also occurred along this fault, consistent with the minor clockwise, vertical-axis rotation of crustal blocks that our paleomagnetic analysis reveals. These observations are consistent with left-lateral slip along the NNE-striking nodal planes of shallow-depth earthquake focal mechanisms in the nearby Gulf of Fonseca (Fig. 5). The abundant and recent deformation in this region, including E-W elongation and possibly trench-parallel right-lateral shear, is consistent with a model in which this region is part of a step-over zone in a major right-lateral offset of the Central American volcanic arc.

DISCUSSION

Forearc Kinematics from GPS

Slip Rate across Salvadoran and Nicaraguan Volcanic Arcs

The new GPS velocity field illustrates several important aspects of the regional deformation. Within El Salvador, the differential motion between GPS sites close to but on opposite sides of the volcanic arc is 9–10 mm yr^{-1} (Fig. 2), parallel to the El Salvador fault zone. This result constitutes a minimum estimate for the long-term slip rate across the volcanic arc. Modeling of the full velocity field accounting for elastic effects gives a best long-term rate of 15 ± 2 mm yr^{-1} relative to the plate interior, comparable to a 11 mm yr^{-1} slip rate estimated from dex-

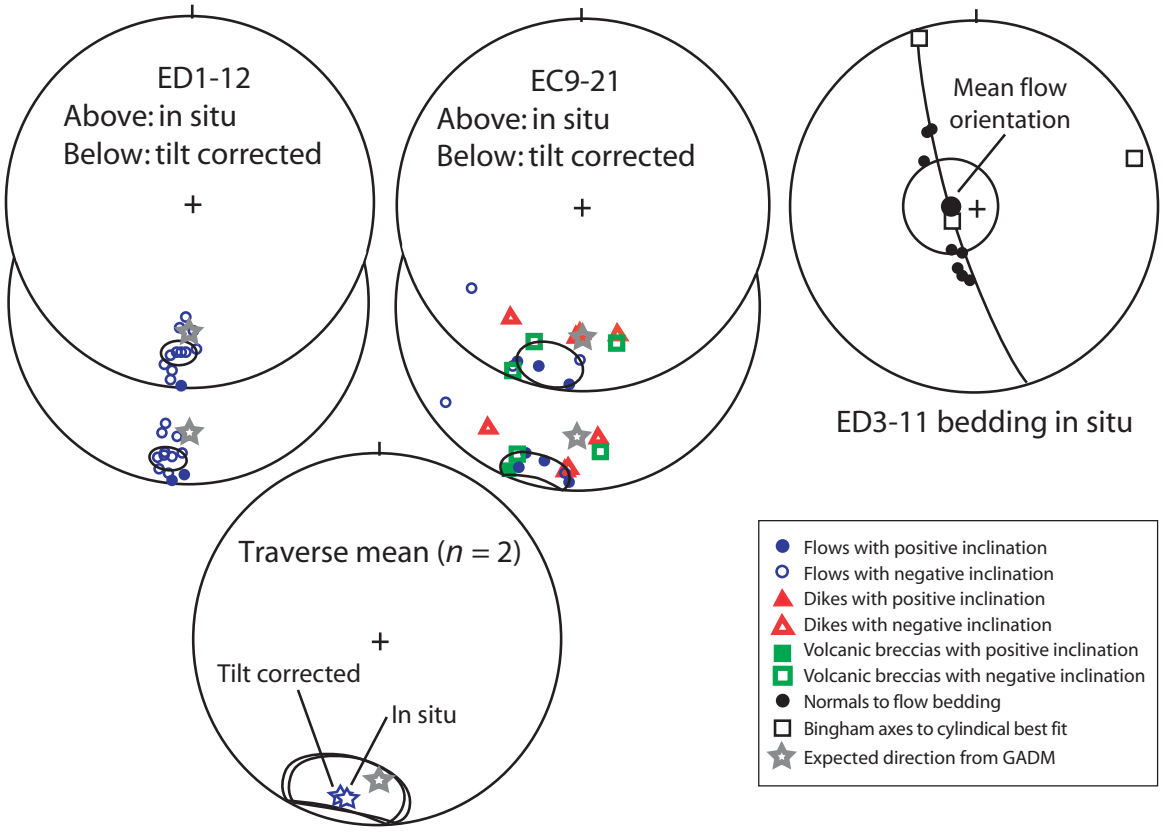

Figure 12. Stereonet plots of bedding orientations and site mean magnetic directions before and after tilt corrections. GADM—Geocentric Axial Dipole Model.

tral offsets of drainages across the El Salvador fault zone (Corti et al., 2005) and to the 10 mm yr^{-1} differential movement of two GPS sites that span the volcanic arc in Guatemala (Lyon-Caen et al., 2006). All of these indicate that the long-term movement of the Salvadoran forearc exceeds 10 mm yr^{-1} relative to the Caribbean plate, which is faster than expected given the absence of oblique convergence across the subduction zone offshore.

The slip rate in Nicaragua is less well determined, mainly due to greater uncertainty in the Nicaraguan station velocities. Our modeling suggests a best long-term rate of 17 ± 2 mm yr^{-1} (Fig. 2), which is insignificantly faster than that for the Salvadoran forearc.

Implications for the Forces that Drive and Resist Forearc Motion

The GPS and structural observations described here highlight two unusual aspects of the study area that may hold useful information about the forces responsible for driving motion of the Nicaraguan and Salvadoran forearcs. First, the absence of oblique subduction beneath the translating Salvadoran forearc precludes partitioning of oblique subduction as the driving force for its trench-parallel motion, the usual explanation for why forearcs move along trenches (e.g., Avé Lallemant and Guth, 1990; Beck, 1991; McCaffrey, 1992). Second, the kinematic evidence that the Nicaraguan and Salvadoran forearcs comprise a single undeforming forearc sliver is surprising given that the obliquity of Cocos plate subduction changes by 20°–25° from Nicaragua to El Salvador. Comparable changes in the angle of subduction obliquity elsewhere are associated with along-strike forearc elongation and shortening (e.g., Avé Lallemant and Guth, 1990; Fossen and Tikoff, 1998). Other factors may therefore influence forearc kinematics in this region and, by inference, other areas.

We suggest that the weak frictional coupling of the Cocos plate subduction interface offshore from much of Central America (Lyon-Caen et al., 2006; Correa-Mora et al., 2009; LaFemina et al., 2009) is central to understanding the forces that drive and resist the trench-parallel motion of the Central American forearc. Weak or no coupling across the subduction interface implies that the subducting Cocos plate imparts little or no traction on the base of the Central American forearc, either parallel or perpendicular to the trench. By implication, partitioning of the observed oblique subduction beneath the coast of southeastern Nicaragua (DeMets, 2001; LaFemina et al., 2009) is unlikely to drive the trench-parallel motion of the Nicaraguan forearc, as advocated by DeMets (2001), unless the subduction coupling offshore from Nicaragua is significantly higher over longer time periods than implied by GPS measurements over the past decade.

Other forces must therefore be invoked to move the Nicaraguan and Salvadoran forearcs, possibly at the trailing edge of the forearc in Costa Rica (Fig. 4) or along the leading edge of the forearc in Guatemala. Both are considered in the following paragraphs.

From modeling of GPS measurements in Costa Rica and Nicaragua, LaFemina et al. (2009) proposed that the ongoing collision of the Cocos Ridge with the Middle America subduction zone off the coast of Costa Rica drives the trench-parallel motions of the Costa Rican, Nicaraguan, and Salvadoran forearcs. In this model, the buoyant Cocos Ridge indents the western edge of the Caribbean plate and induces lateral, northwestward escape of the Costa Rican forearc, which in turn drives northwestward movement of the Nicaraguan forearc.

Figure 4 shows how the motions of the Salvadoran and possibly Guatemalan forearcs might also be distant effects of this collision. The weak frictional coupling across the subduction interface at the base of the Central America forearc sliver plays a key role by leaving these forearcs relatively free to translate along the trench in response to a push from behind. DeMets (2002) and LaFemina et al. (2009) both showed that thrust earthquake slip directions offshore from the Nicaragua, El Salvador, and eastern Guatemala forearcs are deflected systematically clockwise from the Cocos-Caribbean slip direction, as expected if these forearcs were escaping northwestward or westward from the Cocos Ridge collision zone. The partially partitioned oblique subduction off the coast of southeastern Nicaragua previously described and interpreted by DeMets (2001) as the cause of trench-parallel translation of the Nicaraguan forearc may reflect forearc escape.

The available data do not exclude a model in which partitioning of obliquely convergent Cocos-Caribbean plate motion offshore from Costa Rica, where coupling across the subduction interface is higher (Norabuena et al., 2004; LaFemina et al., 2009), may contribute to the trench-parallel motions of the Nicaraguan and hence Salvadoran forearcs. Whatever the driving force, low frictional coupling across the bases of the Nicaragua and Salvadoran forearcs may play a critical role in allowing the two forearcs to translate as a rigid or quasi-rigid crustal sliver.

Translation of the Central America forearc may also be driven by a pull on its leading edge in eastern and central Guatemala (Fig. 4). Malfait and Dinkelman (1972) and Burkart (1983) postulated that the western end of the Central American forearc is pinched between the North American and the Cocos plates and may therefore be dragged westward with the North American plate. Rapid westward motion of the western end of the forearc would pull on the trailing Salvadoran and Nicaraguan forearcs, possibly explaining their motions. Extensional structures might then be expected to form in both the Salvadoran and Nicaraguan forearcs. Our GPS measurements, however, show no evidence for significant stretching of the forearc (Fig. 2), and we are unaware of any evidence for large-scale extensional faulting across the entire forearc. Normal faults in the Gulf of Fonseca and southeastern El Salvador (Fig. 6) and along the Nicaraguan and Salvadoran volcanic arcs (Cowan et al., 2002; LaFemina et al., 2002; Corti et al., 2005; Agostini et al., 2006) are localized to offsets of the volcanic arc or changes in its trend. Driving the forearc via a "pull" on its leading edge thus seems physically implausible given both the weakness of continental crust under tension and the lack of any supporting geodetic or structural evidence.

Gulf of Fonseca

Our second objective was to determine how motion is transferred from faults in central Nicaragua to faults in central El Salvador across the Gulf of Fonseca, where the volcanic arc is offset and changes trend. The geodetic, seismologic, structural, and paleomagnetic data described here and the velocities of two GPS sites from eastern El Salvador provide a strong basis for testing between alternative hypotheses for how the motion is transferred (Fig. 3). Two of these models, the fault-jog and fault-termination models (Figs. 3A and 3C), postulate that faults in the offset volcanic arcs are connected by one or more N-NW–striking faults that presumably sole onto a single master fault, comprising a relatively narrow zone of deformation. The fault termination model also allows for differential movement between the Salvadoran and Nicaraguan forearc slivers offshore. In contrast, the pull-apart model (Fig. 3B) postulates that slip is transferred gradually between the Nicaraguan and Salvadoran volcanic arc faults by a series of intervening structures that are bounded by strike-slip faults at their northern and southern edges. The eastern edge of the pull-apart is defined by the Gulf of Fonseca, with prominent normal faulting and low elevations. The western edge of the pull-apart is defined by a lack of distributed faulting observed in DEM, presence of magmatic centers that do not follow a linear trend, and consistency of GPS movements south of the El Salvador fault zone outside (west) of the pull-apart; the exact orientation and position of the western boundary is not precisely known. The location of the southern boundary of the pull-apart structure occurs offshore.

The GPS, seismic, and structural data favor a model in which deformation across a broad pull-apart zone in eastern El Salvador and the Gulf of Fonseca gradually transfers dextral shear across volcanic arc faults in Nicaragua inland to the volcanic arc faults of El Salvador (Fig. 3B). Earthquake focal mechanisms in and near the Gulf of Fonseca are evidence that dextral E-W strike-slip earthquakes and/or bookshelf faulting via left-lateral slip along N-trending faults accommodate deformation in the step-over. Abundant evidence shows that this strike-slip faulting is accompanied by active extension, despite the absence of normal-faulting earthquake focal mechanisms in this zone. Soil layers and young (430 ka and 1114 ka) volcanic units are offset by N-S–trending normal faults that are ubiquitous in eastern El Salvador (Fig. 6), demonstrating the youth of those faults. North-south–trending normal faults also clearly appear on islands in the Gulf of Fonseca (Fig. 6), together defining a zone of distributed normal faulting that is ~60 km wide from east-to-west and ~40 km wide north-to-south. Within this deforming zone, GPS stations JUCU and SAIN (Fig. 5) have respectively faster eastward motions relative to the Salvadoran forearc, which are also consistent with distributed E-W–directed elongation across this region.

We therefore propose that much of eastern El Salvador belongs to a pull-apart zone that includes the Gulf of Fonseca, which we herein name the Fonseca pull-apart. Funk et al. (2009) independently reached a similar conclusion from their analysis of topography around the Gulf of Fonseca and two marine seismic lines in the gulf. The precise geographic limits of the Fonseca pull-apart are unknown. Reconnaissance field work done in easternmost El Salvador indicates that the El Salvador fault zone described by Corti et al. (2005) does not continue eastward to the border with Honduras. In this locale, we found no geomorphic expression of a large fault, nor was faulting as obvious as we observed in the outcrops in Sierra de Jucuaran farther south, where we surveyed the Chirilagua fault. Although we were unable to locate the northern margin of the Fonseca pull-apart, one or more structures east of the El Salvador fault zone must connect eastward to active faults in the Gulf of Fonseca (Fig. 5) and remain to be discovered. The southern margin of the Fonseca pull-apart is likely to be offshore and may be marked by a line of small earthquakes west of the Gulf of Fonseca or possibly by the southwestern limit of the Nicaragua Depression imaged in the gulf by Funk et al. (2009).

Our detailed structural study of the Chirilagua fault within the Fonseca pull-apart provides useful additional information about the pull-apart, albeit at a much smaller scale than our other data. The N-S strike of the fault is consistent with the regional normal-fault strikes and geodetic evidence for E-W extension in this area. The Lidar data show that the downdip movement along the fault is dominant (Fig. 9B), as expected for a steeply dipping normal fault, but they also reveal numerous slickenlines consistent with a more recent phase of left-lateral oblique slip and additional but fewer slickenlines consistent with right-lateral oblique slip. Crosscutting relationships between the slickenlines formed by downdip and left oblique slip (Fig. 10) require that downdip movement occurred first. The relative timing of the more weakly expressed phase of oblique right-lateral slip is unknown.

Our paleomagnetic analysis indicates that ~10° of clockwise rotation may have occurred

in the relatively young footwall rocks (ca. 1 Ma or younger) of the Chirilagua fault (Fig. 12). Although the uncertainties and small amount of rotation do not allow us to establish definitely that block rotation is occurring, clockwise rotation of fault-bounded blocks within the Fonseca pull-apart is consistent with the kinematically required E-W dextral shear across the pull-apart due to the motion of the forearc (Figs. 3 and 4). In addition, left-lateral oblique slip is consistent with that expected if the fault-bounded blocks in the Fonseca pull-apart undergo bookshelf faulting in response to dextral shear across its bounding faults, as also appears to occur in the Managua graben of central Nicaragua (LaFemina et al., 2002).

On the basis of these observations, we propose that deformation within the Fonseca pull-apart consists of E-W elongation of an ~60-km-wide extensional zone, possibly with some bookshelf faulting. The gradual transfer of motion from the forearc faults that bound the pull-apart to the north and south implies that slip rates on the El Salvador fault zone decrease to the east along the eastward continuation of the fault proposed by Martínez-Díaz et al. (2004), as illustrated in Figure 5. This motion may be transferred via faults within the pull-apart to a proposed right-lateral strike-slip fault that bounds the southern edge of the pull-apart and continues eastward across the Gulf of Fonseca to the Nicaraguan volcanic arc. Funk et al. (2009) found evidence in marine seismic lines within the gulf for one such fault cutting across the gulf, although they interpreted this structure as the southern edge of the volcanic graben. Although the location of deformation is presumably primarily dictated by where the volcanic arc is offset, preexisting structures may also influence the location, geometry, and style of present deformation.

LIMITATIONS OF PRESENT STUDY

Although our work represents a step forward in understanding the kinematics and geologically recent deformation of the Salvadoran forearc and its intersection with the Nicaraguan forearc across the Gulf of Fonseca, many uncertainties remain. Our treatment of the Nicaraguan volcanic arc as a simple strike-slip system is clearly oversimplified in light of the evidence described by Cowan et al. (2002), La Femina et al. (2002), Cailleau et al.,(2007), and Funk et al. (2009) that dextral shear across the volcanic arc is accommodated across a 10–20-km-wide deforming zone for much of its length. Significant questions also remain about how motion along faults in the Nicaraguan volcanic arc is transferred across the Gulf of Fonseca to the El Salvador fault zone. Further work is also needed to better understand how approximately E-W elongation across much of Central America inland from the Salvadoran and Guatemalan volcanic arcs (Lyon-Caen et al., 2006; Rodriguez et al., 2009) may influence our model-based estimate of the forearc motions. Finally, large uncertainties in the velocities for most stations in Nicaragua are an important limiting factor in our ability to detect any motion between the Nicaraguan and Salvadoran forearcs. Ongoing measurements at GPS stations throughout the region should soon help us to better understand the regional tectonics and seismic hazard.

CONCLUSIONS

GPS velocities for sites in El Salvador, southern Honduras, and Nicaragua indicate that the Nicaraguan and Salvadoran forearcs move together at rates of 15 ± 2 mm yr^{-1} to the WNW-NW relative to the Caribbean plate. Offshore from El Salvador, the Cocos plate subducts in a direction orthogonal to the trench, thereby ruling out partitioning of oblique subduction as a possible explanation for the trench-parallel motion of the Salvadoran forearc. Offshore from Nicaragua, observed partial partitioning of up to ~25 degrees of oblique Cocos plate convergence could be evidence that oblique convergence drives motion of the Nicaragua forearc. However, GPS measurements in both El Salvador and Nicaragua clearly indicate that the subducting Cocos plate imposes little or no traction on the base of either forearc and therefore may be incapable of influencing their motions. We therefore infer that the northwestward motion of the Nicaraguan forearc is driven by the collision of the Cocos Ridge with the edge of the continent in Costa Rica, as suggested by LaFemina et al. (2009). We further infer that the Salvadoran forearc is pushed to the WNW along the trench by the Nicaraguan forearc, with both forearcs free to move due to the weak coupling along their bases.

The slower-than-expected motions of two GPS sites in southeastern El Salvador are consistent with regional- and local-scale seismic and structural evidence for broadly distributed deformation across an ~60-km-wide extensional step-over of the volcanic arc in this region and the Gulf of Fonseca. Our analysis of 10-m-resolution digital elevation models and reconnaissance structural data from this region reveals that normal faults oriented at a high angle to the trench accommodate active E-W elongation within the Fonseca pull-apart zone. Structural measurements and Lidar imagery from the superbly exposed Chirilagua fault in the step-over zone and 33 paleomagnetic sites from two transects of the fault footwall indicate that E-W elongation and possibly bookshelf faulting dominate the deformation within the fault step-over. Late left-lateral, oblique slip motion on the Chirilagua fault and clockwise rotation of the fault footwall are indications that a component of bookshelf faulting is associated with the fault step-over. The young ages of volcanic unit offset by normal faults in SE El Salvador demonstrate that trench-parallel elongation of the forearc is ongoing.

ACKNOWLEDGMENTS

The Global Positioning System (GPS) networks in El Salvador and Honduras are operated as collaborative efforts by Servicio Nacional de Estudios Territoriales in El Salvador, the Universidad Nacional Autónoma de Honduras in Tegucigalpa, and the University of Wisconsin–Madison. We thank Comision Permanente de Contingencias of Honduras for logistical support in the early stages of this project. This work was funded by National Science Foundation (NSF) grants EAR-0309839 and EAR-0538131 (to DeMets and Tikoff). GPS observations in Nicaragua were funded by EAR-0538135 (to Mattioli). Figures were produced using Generic Mapping Tools software (Wessel and Smith, 1991). Paleomagnetic analysis was supported by the University of New Mexico (UNM) paleomagnetism laboratory and Lidar data acquisition by the UNM Lidar laboratory. We thank Brian Jicha for assistance with the argon age dating. We thank Tim Dixon, Pete LaFemina, and Kip Hodges for advice and comments that significantly improved the original manuscript.

REFERENCES CITED

Agostini, S., Corti, G., Doglioni, C., Carminati, E., Innocenti, F., Tonarini, S., Manetti, P., Di Vincenzo, G., and Montanari, D., 2006, Tectonic and magmatic evolution of the active volcanic front in El Salvador: Insight into the Berlin and Ahuachapan geothermal areas: Geothermics, v. 35, p. 368–408, doi: 10.1016/j.geothermics.2006.05.003.

Alvarado, D., 2008, Crustal Deformation of the Salvadoran-Nicaraguan Forearc at the Gulf of Fonseca: A Multidisciplinary Tectonic Study [M.S. thesis]: Madison, University of Wisconsin, 113 p.

Angelier, J., Bergerat, F., Dauteuil, O., and Villemin, T., 1997, Effective tension-shear relationships in extensional fissure swarms: Axial rift zone on northeastern Iceland: Journal of Structural Geology, v. 19, p. 673–685, doi: 10.1016/S0191-8141(96)00106-X.

Avé Lallemant, H.G., and Guth, L.R., 1990, Role of extensional tectonics in exhumation of eclogites and blueschists in an oblique subduction setting, northeastern Venezuela: Geology, v. 18, p. 950–953, doi: 10.1130/0091-7613(1990)018<0950:ROETIE>2.3.CO;2.

Avşar, U., and Isseven, T., 2009, Regional clockwise rotation of the Armutlu Peninsula, western Turkey, resolved from palaeomagnetic study of Eocene volcanics: Tectonophysics, v. 475, p. 415–422, doi: 10.1016/j.tecto.2009.05.021.

Bassin, C., Laske, G., and Masters, G., 2000, The current limits of resolution for surface wave tomography in North America: Eos (Transactions, American Geophysical

Union), v. 81, no. 48, Fall Meeting supplement, abstract S12A-03.

Beck, M.E., 1991, Coastwise transport reconsidered: Lateral displacements in oblique subduction zones, and tectonic consequences: Physics of the Earth and Planetary Interiors, v. 68, p. 1–8, doi: 10.1016/0031-9201(91)90002-Y.

Burkart, B., 1983, Neogene North American–Caribbean plate boundary: Offset along the Polochic fault: Tectonophysics, v. 99, p. 251–270, doi: 10.1016/0040-1951(83)90107-5.

Butler, R.F., 1992, Paleomagnetism: Oxford, Blackwell Scientific, 319 p.

Cailleau, B., La Femina, P., and Dixon, T., 2007, Stress accumulation between volcanoes: An explanation for intra-arc earthquakes in Nicaragua?: Geophysical Journal International, v. 169, p. 1132–1138, doi: 10.1111/j.1365-246X.2007.03353.x.

Carr, M.J., and Stoiber, R.E., 1977, Geologic setting of some destructive earthquakes in Central America: Geological Society of America Bulletin, v. 88, p. 151–156, doi: 10.1130/0016-7606(1977)88<151:GSOSDE>2.0.CO;2.

Correa-Mora, F., DeMets, C., Cabral-Cano, E., Marquez-Azua, B., and Diaz-Molina, O., 2008, Interplate coupling and transient slip along the subduction interface beneath Oaxaca, Mexico: Geophysical Journal International, v. 175, p. 269–290, doi: 10.1111/j.1365-246X.2008.03910.x.

Correa-Mora, F., DeMets, C., Alvarado, D., Turner, H.L., Mattioli, G., Hernandez, D., Pullinger, C., Rodriguez, M., and Tenorio, C., 2009, GPS-derived coupling estimates for the Central America subduction zone and volcanic arc faults: El Salvador, Honduras, and Nicaragua: Geophysical Journal International, v. 179, p. 1279–1291, doi: 10.1111/j.1365-246X.2009.04371.x.

Corti, G., Carminati, E., Mazzarini, F., and Garcia, M.O., 2005, Active strike-slip faulting in El Salvador, Central America: Geology, v. 33, p. 989–992, doi: 10.1130/G21992.1.

Cowan, H., Prentice, C., Pantosti, D., de Martini, P., Strauch, W., and Workshop Participants, 2002, Late Holocene earthquakes on the Aeropuerto fault, Managua, Nicaragua: Bulletin of the Seismological Society of America, v. 92, p. 1694–1707, doi: 10.1785/0120010100.

DeMets, C., 2001, A new estimate for present-day Cocos-Caribbean plate motion: Implications for slip along the Central American volcanic arc: Geophysical Research Letters, v. 28, p. 4043–4046, doi: 10.1029/2001GL013518.

DeMets, C., 2002, Reply to comment on "A new estimate for present-day Cocos-Caribbean plate motion: Implications for slip along the Central American volcanic arc" by Marco Guzman-Speziale and Juan Martin Gomez: Geophysical Research Letters, v. 29, doi: 10.1029/2002GL015384.

DeMets, C., Mattioli, G., Jansma, P., Rogers, R., Tenorio, C., and Turner, H.L., 2007, Present motion and deformation of the Caribbean plate: Constraints from new GPS geodetic measurements from Honduras and Nicaragua, *in* Mann, P., ed., Geologic and Tectonic Development of the Caribbean Plate in Northern Central America: Geological Society of America Special Paper 428, p. 21–36, doi: 10.1130/2007.2428(02).

Doblas, M., 1998, Slickenline kinematic indicators: Tectonophysics, v. 295, p. 187–197, doi: 10.1016/S0040-1951(98)00120-6.

Ferrill, D.A., Stamatakos, J.A., and Sims, D., 1999, Normal fault corrugation: Implications for growth and seismicity of active normal faults: Journal of Structural Geology, v. 21, p. 1027–1038, doi: 10.1016/S0191-8141(99)00017-6.

Fitch, T.J., 1972, Plate convergence, transcurrent faults, and internal deformation adjacent to Southeast Asia and the western Pacific: Journal of Geophysical Research, v. 77, p. 4432–4460, doi: 10.1029/JB077i023p04432.

Fossen, H., and Tikoff, B., 1998, Extended models of transpression and transtension, and application to tectonic settings, *in* Holsworth, R.E., Strachan, R.A., and Dewey, J.F., eds., Continental Transpressional and Transtensional Tectonics: Geological Society, London, Special Publication 135, p. 15–33, doi: 10.1144/GSL.SP.1998.135.01.02.

Funk, J., Mann, P., McIntosh, K., and Stephens, J., 2009, Cenozoic tectonics of the Nicaraguan depression, Nicaragua, and Median Trough, El Salvador, based on seismic-reflection profiling and remote-sensing data: Geological Society of America Bulletin, v. 121, p. 1491–1521, doi: 10.1130/B26428.1.

Geist, E.L., Childs, J.R., and Scholl, D.W., 1988, The origin of summit basins of the Aleutian Ridge: Implications for block rotation of an arc massif: Tectonophysics, v. 7, p. 327–341.

Grant, J.V., and Kattenhorn, S.A., 2004, Evolution of vertical faults at an extensional plate boundary, southwest Iceland: Journal of Structural Geology, v. 26, p. 537–557, doi: 10.1016/j.jsg.2003.07.003.

Jarrard, R.D., 1986, Relations among subduction parameters: Reviews of Geophysics, v. 24, p. 217–284, doi: 10.1029/RG024i002p00217.

Jones, C.H., 2002, User-driven integrated software lives: "PaleoMag" Paleomagnetics analysis on the Macintosh: Computers & Geosciences, v. 28, p. 1145–1151, doi: 10.1016/S0098-3004(02)00032-8.

Kaven, J.O., and Martel, S.T., 2007, Growth of surface-breaching normal faults as a three-dimensional fracturing process: Journal of Structural Geology, v. 29, p. 1463–1476, doi: 10.1016/j.jsg.2007.05.007.

Kimura, G., 1986, Oblique subduction and collision: Forearc tectonics of the Kuril arc: Geology, v. 14, p. 404–407, doi: 10.1130/0091-7613(1986)14<404:OSACFT>2.0.CO;2.

LaFemina, P.C., Dixon, T.H., and Strauch, W., 2002, Bookshelf faulting in Nicaragua: Geology, v. 30, p. 751–754, doi: 10.1130/0091-7613(2002)030<0751:BFIN>2.0.CO;2.

LaFemina, P.C., Dixon, T.H., Govers, R., Norabuena, E., Turner, H., Saballos, A., Mattioli, G., Protti, M., and Strauch, W., 2009, Forearc motion and Cocos Ridge collision in Central America: Geochemistry Geophysics Geosystems, v. 10, p. Q05S14, doi: 10.1029/2008GC002181.

Luyendyk, B.P., 1991, A model for Neogene crustal rotations, transtension, and transpression in southern California: Geological Society of America Bulletin, v. 103, p. 1528–1536, doi: 10.1130/0016-7606(1991)103<1528:AMFNC>2.3.CO;2.

Lyon-Caen, H., Barrier, E., Lasserre, C., Franco, A., Arzu, I., Chiquin, M., Chiquin, L.M., Duquesnoy, T., Flores, O., Galicia, O., Luna, J., Molina, E., Porras, O., Requena, J., Robles, V., Romero, J., and Wolf, R., 2006, Kinematics of the North American–Caribbean–Cocos plates in Central America from new GPS measurements across the Polochic-Motagua fault system: Geophysical Research Letters, v. 33, p. L19309, doi: 10.1029/2006GL027694.

Malfait, B.T., and Dinkelman, M.G., 1972, Circum-Caribbean tectonic and igneous activity and the evolution of the Caribbean plate: Geological Society of America Bulletin, v. 83, p. 251–271, doi: 10.1130/0016-7606(1972)83[251:CTAIAA]2.0.CO;2.

Markley, M., and Tikoff, B., 2002, Matchsticks on parade; vertical axis rotation in oblique divergence: Journal of Geophysical Research, v. 107, doi: 10.1029/2002JB001826.

Martel, S.J., and Langley, J.S., 2006, Propagation of normal faults to the surface in basalt, Koae fault system, Hawaii: Journal of Structural Geology, v. 28, p. 2123–2143, doi: 10.1016/j.jsg.2005.12.004.

Martínez-Díaz, J.J., Álvarez-Gómez, J.A., Benito, B., and Hernandez, D., 2004, Triggering of destructive earthquakes in El Salvador: Geology, v. 32, p. 65–68, doi: 10.1130/G20089.1.

McCaffrey, R., 1992, Oblique plate convergence, slip vectors, and forearc deformation: Journal of Geophysical Research, v. 97, p. 8905–8915, doi: 10.1029/92JB00483.

McCaffrey, R., 1996, Estimates of modern arc-parallel strain rates in forearcs: Geology, v. 24, p. 27–30, doi: 10.1130/0091-7613(1996)024<0027:EOMAPS>2.3.CO;2.

Muffler, L.J.P., Clynne, M.A., and Champion, D.E., 1994, Late Quaternary normal faulting of the Hat Creek Basalt, northern California: Geological Society of America Bulletin, v. 106, p. 195–200.

Norabuena, E., Dixon, T.H., Schwartz, S., DeShon, H., Newman, A., Protti, M., Gonzalez, V., Dorman, L., Flueh, E.R., Lundgren, P., Pollitz, F., and Sampson, D., 2004, Geodetic and seismic constraints on some seismogenic zone processes in Costa Rica: Journal of Geophysical Research, v. 109, p. B11403, doi: 10.1029/2003JB002931.

Peacock, D.C.P., and Parfitt, E.A., 2002, Active relay ramps and normal fault propagation on Kilauea Volcano, Hawaii: Journal of Structural Geology, v. 24, p. 729–742, doi: 10.1016/S0191-8141(01)00109-2.

Petronis, M.S., Geissman, J.W., Oldow, J.O., and McIntosh, W.C., 2002, Paleomagnetic and $^{40}Ar/^{39}Ar$ geochronologic data bearing on the structural evolution of the Silver Peak extensional complex, west-central Nevada: Geological Society of America Bulletin, v. 114, p. 1108–1130.

Renne, P.R., Swisher, C.C., Deino, A.L., Karner, D.B., Owens, T.L., and DePaolo, D.J., 1998, Intercalibration of standards, absolute ages, and uncertainties in $^{40}Ar/^{39}Ar$ dating: Chemical Geology, v. 145, p. 117–152, doi: 10.1016/S0009-2541(97)00159-9.

Rodriguez, M., DeMets, C., Rogers, R., Tenorio, C., and Hernandez, D., 2009, A GPS and modeling study of deformation in northern Central America: Geophysical Journal International, v. 178, p. 1733–1754, doi: 10.1111/j.1365-246X.2009.04251.x.

Schmalzle, G., Dixon, T., Malservisi, R., and Govers, R., 2006, Strain accumulation across the Carrizo segment of the San Andreas fault, California: Impact of laterally varying crustal properties: Journal of Geophysical Research, v. 111, p. B05403, doi: 10.1029/2005JB003843.

Steiger, R.H., and Jäger, E., 1977, Subcommission on geochronology: Convention on the use of decay constants in geo- and cosmochronology: Earth and Planetary Science Letters, v. 36, p. 359–362, doi: 10.1016/0012-821X(77)90060-7.

Turner, H.L.I., LaFemina, P., Saballos, A., Mattioli, G.S., Jansma, P.E., and Dixon, T., 2007, Kinematics of the Nicaraguan forearc from GPS geodesy: Geophysical Research Letters, v. 34, p. L02302, doi: 10.1029/2006GL027586.

Wawrzyniec, T.F., Geissman, J.W., Melker, M.D., and Hubbard, M., 2002, Dextral shear along the eastern margin of the Colorado plateau: A kinematic link between Laramide contraction and Rio Grande rifting (ca. 75–13 Ma): Journal of Geology, v. 110, p. 305–324.

Wessel, P., and Smith, W.H.F., 1991, Free software helps map and display data: Eos (Transactions, American Geophysical Union), v. 72, p. 441–446, doi: 10.1029/90EO00319.

White, I.R., and Crider, J.G., 2006, Extensional fault-propagation folds: Mechanical models and observations from the Modoc Plateau, northeastern California: Journal of Structural Geology, v. 28, p. 1352–1370, doi: 10.1016/j.jsg.2006.03.028.

White, R.A., 1991, Tectonic implications of upper-crustal seismicity in Central America, *in* Slemmons, D.B., Engdahl, E.R., Zoback, M.D., and Blackwell, D.D., eds., Neotectonics of North America: Boulder, Colorado, Geological Society of America, Decade of North American Geology Map 1, p. 323–328.

White, R.A., and Harlow, D.H., 1993, Destructive upper-crustal earthquakes of Central America since 1900: Bulletin of the Seismological Society of America, v. 83, p. 1115–1142.

Wiesemann, G., 1975, Remarks on the geologic structure of the Republic of El Salvador, Central America: Mitteilungen der Geologisch-Paläontologische Institut, University of Hamburg, v. 44, p. 557–574.

MANUSCRIPT RECEIVED 9 APRIL 2010
REVISED MANUSCRIPT RECEIVED 6 SEPTEMBER 2010
MANUSCRIPT ACCEPTED 8 SEPTEMBER 2010

Printed in the USA